

Synthesis and Coordination Chemistry of Chelate Ligands Containing Cyclopentadienyl, Indenyl and Fluorenyl Donors – Diastereoselectivity and NMR Structure Analysis

Joachim Vogelgesang,^[a] Axel Frick,^[a] Gottfried Huttner,^{*[a]} and Peter Kircher^[a]

Dedicated to Prof. Dr. Heinrich Vahrenkamp on the occasion of his 60th birthday

Keywords: Cyclopentadienes / Tripodal ligands / NMR spectroscopy / Distance geometry / Ruthenium / Phosphorus

The functionalised oxetane $\text{O}(\text{CH}_2)_2\text{C}(\text{CH}_2\text{Br})(\text{CH}_2\text{OMs})$ (**1**) is transformed into *tripod* ligands $\text{ROCH}_2\text{C}(\text{CH}_2\text{PPh}_2)(\text{CH}_2\text{PR}'_2)(\text{CH}_2\text{Cp}^\#)$ ($\text{R} = \text{H}, \text{SiMe}_3$; $\text{R}' = \text{Ph}, \text{Et}$; $\text{Cp}^\# = \text{indenyl}, \text{fluorenyl}$) (**4**) in a few steps. Epichlorohydrin $\text{O}(\text{CH}_2)\text{CH}(\text{CH}_2\text{Cl})$ (**5**) allows for diastereoselective one-pot syntheses of the Cp-functionalised chelate ligands $(\text{Cp}^\#\text{CH}_2)\text{C}(\text{H})\text{OH}(\text{CH}_2\text{PPh}_2)$ ($\text{Cp}^\# = \text{Cp}, \text{indenyl}, \text{fluorenyl}$) (**6**). The SiMe_3 -protected derivatives of these ligands react with $\text{RuCl}_2(\text{PPh}_3)_3$ to produce $\{\text{Me}_3\text{SiOCH}(\text{CH}_2-\eta^1\text{-PPh}_2)(\text{CH}_2-\eta^5\text{-Cp}^\#)\text{Ru}(\text{PPh}_3)(\text{Cl})\}$ ($\text{Cp}^\# = \text{Cp}, \text{indenyl}$) (**15**) with high diastereoselective preference. With the same start-

ing material, *tripod* ligands **4** form $\text{Me}_3\text{SiOCH}_2\text{C}(\text{CH}_2-\eta^1\text{-PPh}_2)(\text{CH}_2-\eta^1\text{-PR}_2)(\text{CH}_2-\eta^5\text{-Indenyl})\text{RuCl}$ ($\text{R} = \text{Ph}, \text{Et}$) (**16**). As shown by complete NMR spectroscopy based structure analyses (DG methods) of **16**, the formation of **16** ($\text{R} = \text{Et}$) is diastereoselective. The only diastereomer which is observed is the one in which the PEt_2 donor and the phenylene part of the indenyl ligand are juxtaposed. In addition to quantitative NMR spectroscopy structure analyses, traditional analytical techniques, including X-ray analyses, were used to confirm the results.

Introduction

Cyclopentadienyl ligands which are linked to additional donor groups by side-chains of appropriate lengths are a special class of chelate ligands and hold quite some promise in catalytic applications. Whereas the chemistry of *ansa* Cp ligands, so elegantly developed by H. Brintzinger and his group,^[1] has boomed in recent years, the chemistry of Cp-based chelate ligands bearing functionalities other than Cp groups is only in its early state of development. This is especially surprising in the case of Cp derivatives containing additional phosphane donor groups, since the chemistry of $\text{CpM}(\text{PR}_3)_n$ metal templates is so well developed. The only possible reason for this fact appears to be the lack of suitable methods for the synthesis of the ligands. It has been shown that tripodal ligands $\text{CH}_3\text{C}(\text{CH}_2\text{PR}_2)(\text{CH}_2\text{PR}'_2)(\text{CH}_2\text{Cp}^\#)$ ($\text{Cp}^\# = \text{Cp}, \text{indenyl}, \text{fluorenyl}$) are accessible by different routes^[2] and some coordination chemistry of such ligands has been reported.^[3]

Since it has been shown that *tripod* ligands $\text{H}_3\text{CC}(\text{CH}_2\text{X})(\text{CH}_2\text{Y})(\text{CH}_2\text{Z})$ ($\text{X}, \text{Y}, \text{Z} = \text{donor groups}$ with at least one of them being a Cp derivative) are accessible via appropriately functionalised oxetanes in fair yields,^[2] the development of the synthesis of hydroxy-functionalised *tripod* ligands $(\text{HOCH}_2)\text{C}(\text{CH}_2\text{PR}_2)(\text{CH}_2\text{PR}'_2)(\text{CH}_2\text{Cp}^\#)$ via oxetane precursors appears to be worthwhile. In this paper ligands of this type ($\text{Cp}^\# = \text{indenyl}, \text{fluorenyl}$;

$\text{PR}_2, \text{PR}'_2 = \text{PPh}_2, \text{PEt}_2$) (**3, 4**) as well as some of their coordination chemistry, are described.

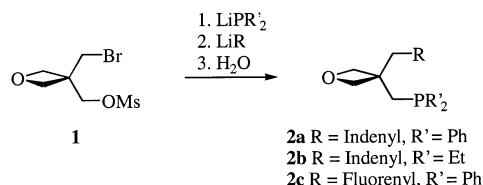
Yet another way to hydroxy-functionalised chelate ligands containing phosphorus donor groups and $\text{Cp}^\#$ ligands linked by a three-carbon chain may be based on the use of epichlorohydrin as the starting material. It has been shown that the enantioselective synthesis of bidentate and tridentate chelate ligands containing up to three different phosphorus donors $\text{HC}(\text{CH}_2\text{PR}_2)(\text{CH}_2\text{PR}'_2)(\text{OPR}''_2)$ may be achieved in this way.^[4] In this paper we show that $\text{Cp}^\#$ donor groups may also be introduced, leading to compounds $\text{HC}(\text{CH}_2\text{Cp}^\#)(\text{CH}_2\text{PPh}_2)(\text{OPPh}_2)$ (**12**) and $\text{ROCH}(\text{CH}_2\text{Cp}^\#)(\text{CH}_2\text{PPh}_2)$ (**6, 9**). Some coordination compounds of these novel ligands are also described.

Results and Discussion

Ligand Syntheses

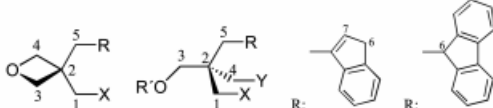
Starting from Neopentane Derivatives

The functionalised oxetane **1**, which has been shown to undergo selective exchange of its functional groups by two



Scheme 1

^[a] Anorganisch-Chemisches Institut der Universität Heidelberg, Im Neuenheimer Feld 270, 69120 Heidelberg, Germany
Fax: (internat.) + 49-(0)6221/545707
E-mail: g.huttner@indi.aci.uni-heidelberg.de

Table 1. NMR spectroscopic data of compounds **2**–**4**^[a]


No.	R ^[b] X ^[b] Y, R ^[b]	1 ^[c] CH _{2a,b} [2H]	2 ^[c] C _q	3 ^[c] CH _{2a,b} [2H]	4 ^[c] CH _{2a,b} [2H]	5 ^[c] CH _{2a,b} [2H]	6 ^[c] -CH ₂ - (n = 1–2)	7 ^[c] -CH= [1H]	CH aromatic	X	Y
2a	Indenyl PPh ₂ O (Oxetane)	2.93 (d) ² J _{HP} = 2.6 Hz 37.3 (d) ¹ J _{CP} = 15.6 Hz	— 43.1 (d) ² J _{CP} = 15.6 Hz	4.67, 4.77 (2d) ² J _{HH} = 6.0 Hz 82.4 (d) ³ J _{CP} = 11.0 Hz	— — — ³ J _{CP} = 10.6 Hz	3.25 (s) — 35.4 (d) ³ J _{CP} = 10.6 Hz	3.47 (s) [2H] — 38.7 (s) —	6.27 (s) — — —	7.33–7.67 (m) [14H] — 119.7–146.3 —	— — — {–25.6 (s)}	— — — —
2b	Indenyl PEt ₂ O (Oxetane)	2.06 (d) ² J _{HP} = 4.4 Hz 35.2 (d) ¹ J _{CP} = 16.6 Hz	— 42.6 (d) ² J _{CP} = 15.6 Hz	4.58, 4.70 (2d) ² J _{HH} = 5.8 Hz 82.5 (d) ³ J _{CP} = 10.6 Hz	— — — ³ J _{CP} = 11.0 Hz	3.07 (s) — 35.1 (d) ³ J _{CP} = 11.0 Hz	3.41 (s) [2H] — 38.5 (s) —	6.18 (s) — — —	7.25–7.52 (m) [4H] — 119.5–146.3 —	1.06 (m) [6H] 1.46 (m) [4H] 9.9 (d) ² J _{CP} = 12.1 Hz 20.0 (d) ³ J _{CP} = 11.6 Hz {–31.2 (s)}	— — — —
3a	Indenyl PPh ₂ PPh ₂ , H	2.53, 2.63 (2dd) ² J _{HH} = 14.4 Hz ² J _{HP} = 2.8, 3.4 Hz 37.2 (dd) ¹ J _{CP} = 16.6 Hz ³ J _{CP} = 8.8 Hz	— — 44.5 (t) ² J _{CP} = 11.6 Hz	3.66 (s) — 69.5 (t) ³ J _{CP} = 8.4 Hz	2.53, 2.63 (2dd) ² J _{HH} = 14.4 Hz ² J _{HP} = 2.8, 3.4 Hz 37.2 (dd) ¹ J _{CP} = 16.6 Hz ³ J _{CP} = 8.8 Hz	3.09 (s) — — ³ J _{CP} = 8.5 Hz	3.40 (s) [2H] — — 38.6 (s)	6.39 (s) — — —	7.26–7.59 (m) [24H] — 120.3–146.9 —	— — — {–28.4 (s)}	— — — —
3b	Indenyl PPh ₂ PEt ₂ , H	2.57 (d) ² J _{HP} = 3.6 Hz 37.3 (dd) ¹ J _{CP} = 16.3 Hz ³ J _{CP} = 8.4 Hz	— — 43.7 (pt) ² J _{CP} = 11.4 Hz	3.66 (s) — 69.7 (pt) ³ J _{CP} = 8.3 Hz	1.75 (d) ² J _{HP} = 4.8 Hz 35.4 (dd) ¹ J _{CP} = 16.9 Hz ³ J _{CP} = 8.7 Hz	2.96 (s) — 34.8 (pt) ³ J _{CP} = 8.2 Hz	3.39 (s) [2H] — 38.5 (s) —	6.38 (s) — — —	7.21–7.64 (m) [14H] — 120.2–146.9 —	0.91–1.13 (m) [6H] 1.38–1.50 (m) [4H] 9.8 (d) ² J _{CP} = 11.2 Hz 19.9, 20.0 (2d) ¹ J _{CP} = 10.4 Hz {–27.5 (s)} {–35.0 (s)}	— — — —
4a	Indenyl PPh ₂ PPh ₂ , TMS	2.58 (m) 36.7 (dd) ¹ J _{CP} = 17.0 Hz ³ J _{CP} = 10.0 Hz	— 44.2 (t) ² J _{CP} = 12.0 Hz	3.47 (s) 68.8 (pt) ³ J _{CP} = 9.3 Hz	2.58 (m) 36.7 (dd) ¹ J _{CP} = 17.0 Hz ³ J _{CP} = 10.0 Hz	2.96 (s) 34.5 (t) ³ J _{CP} = 8.5 Hz	3.33 (s) [2H] 38.5 (s) —	6.25 (s) — —	7.20–7.60 (m) [24H] — 120.3–147.2 —	— — — {–27.8 (s)}	— — — —
4b	Indenyl PPh ₂ PEt ₂ , TMS	2.60, 2.70 (2dd) ² J _{HH} = 14.0 Hz ² J _{HP} = 3.8, 4.0 Hz 36.3 (dd) ¹ J _{CP} = 16.0 Hz ³ J _{CP} = 9.0 Hz	— — 43.5 (pt) ² J _{CP} = 12.0 Hz	3.55, 3.60 (2d) ² J _{HH} = 9.7 Hz 68.8 (pt) ³ J _{CP} = 9.2 Hz	1.83 (d) ² J _{HP} = 5.0 Hz 34.8 (dd) ¹ J _{CP} = 16.0 Hz ³ J _{CP} = 9.0 Hz	2.99 (s) — 34.4 (pt) ³ J _{CP} = 8.6 Hz	3.40 (s) [2H] — 38.5 (s) —	6.35 (s) — — —	7.23–7.65 (m) [14H] — 120.4–147.3 —	— — 10.0 (d) ² J _{CP} = 11.0 Hz 20.1, 20.2 (2d) ¹ J _{CP} = 11.0 Hz {–27.2 (s)} {–36.1 (s)}	1.10 (m) [6H] 1.44 (m) [4H] — —
2c	Fluorenyl PPh ₂ O (Oxetane)	2.99 (d) ² J _{HP} = 2.2 Hz 36.9 (d) ¹ J _{CP} = 16.6 Hz	— 43.4 (d) ² J _{CP} = 14.1 Hz	4.41, 4.51 (d) ² J _{HH} = 6.1 Hz 83.5 (d) ³ J _{CP} = 11.1 Hz	— — — ³ J _{CP} = 9.1 Hz	2.53 (d) ³ J _{HH} = 7.2 Hz 42.8 (d) ³ J _{CP} = 9.1 Hz	4.07 (t) [1H] ³ J _{HH} = 7.2 Hz 44.8 (s) —	— — — —	7.30–7.86 (m) [18H] — 120.2–147.3 —	— — — {–26.7 (s)}	— — — —
3c	Fluorenyl PPh ₂ PPh ₂ , H	2.39 (m) ² J _{HH} = 14.5 Hz 37.9 (dd) ¹ J _{CP} = 17.0 Hz ³ J _{CP} = 9.2 Hz	— — 44.9 (t) ² J _{CP} = 11.0 Hz	3.39 (m) — 69.7 (t) ³ J _{CP} = 8.2 Hz	2.39 (m) — 37.9 (dd) ¹ J _{CP} = 17.0 Hz ³ J _{CP} = 9.2 Hz	2.72 (d) ³ J _{HH} = 4.6 Hz 39.3 (t) ³ J _{CP} = 8.3 Hz	4.25 (t) ³ J _{HH} = 4.6 Hz 45.7 (s) —	— — — —	7.24–7.86 (m) [28H] — 120.4–148.9 —	— — — {–29.2 (s)}	— — — —
4c	Fluorenyl PPh ₂ PPh ₂ , TMS	2.37 (m) ² J _{HH} = 15.0 Hz 37.4 (dd) ¹ J _{CP} = 16.3 Hz ³ J _{CP} = 10.0 Hz	— — 44.6 (t) ² J _{CP} = 11.3 Hz	3.25 (s) — 69.3 (t) ³ J _{CP} = 9.0 Hz	2.37 (m) — 37.4 (dd) ¹ J _{CP} = 16.3 Hz ³ J _{CP} = 10.0 Hz	2.69 (d) ³ J _{HH} = 6.0 Hz 38.7 (t) ³ J _{CP} = 8.4 Hz	4.20 (m) — 45.6 (s) —	— — — —	7.20–7.85 (m) [28H] — 120.2–149.2 —	— — — {–29.0 (s)}	— — — —

^[a] For ease of comparison the sequence of entries in this table does not follow the numbering scheme; sequence of entries for each compound: ¹H NMR, ¹³C{¹H} NMR, ³¹P{¹H} NMR spectroscopic data are embedded in curly brackets; solvent: CDCl₃; CH_{2a,b} designates CH₂ groups whose protons may be diastereotopic depending on the symmetry of the compound; lines adjacent to individual column entries indicate that signals referring to the columns to which these lines extend are within the range given in each case or are mapped to one and the same signal. — ^[b] This column refers to the composition of the individual compounds with reference to the graphical illustration (Footnote^[c]). — ^[c] Designators of the individual groups as used in the header of the table: see graphics on top of the table.

different PR₂ donors,^[5] has also been shown to allow for the introduction of one phosphorus and one Cp donor.^[6] The reaction of **1** with one equivalent of LiPPh₂ followed by the reaction with one equivalent of LiInd or LiFlu (Ind = indenyl, Flu = fluorenyl) yields compounds **2** after hydrolysis and chromatographic workup (Scheme 1).

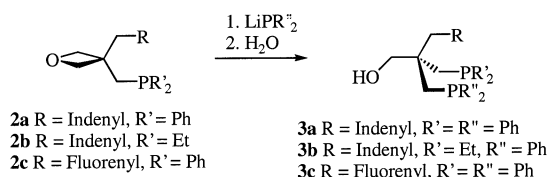
Compounds **2a** (colourless oil) and **2c** (waxy solid) were produced in fair yields (74%/64%) while **2b** (oil) was ob-

tained in a yield of only 10%. The yield of **2b** was lower than that of **2a** because LiPEt₂ is much more basic than LiPPh₂. Instead of replacing the OMs group, PEt₂[–] deprotonated the methyl group of the mesylate function such that upon hydrolysis, the CH₂OMs function was transformed into the CH₂OH function from which the mesylate was prepared.^[7] Similar problems have been observed with tosylate-activating groups where even the *p*-methyl group is acidic

enough to be deprotonated.^[8] The use of phenylsulfonate might be an alternative solution, but has not yet been tested with the problem at hand. The sequence in which the nucleophiles are added in the synthesis of **2** from **1** is important, since selective monosubstitution, which results when LiPR₂ is added first, is not achieved when LiCp[#] is added as the first reagent. Compounds **2** were fully characterised by their spectroscopic and analytical data (Table 1 and Table 10).

All the NMR (¹H, ¹³C, ³¹P) signals, except for those in the aromatic region, have been unambiguously assigned (Table 1). As had already been observed in the synthesis of indenyl-containing *tripod* ligands,^[2a] the indenyl residue was selectively bonded at its 3-position.^[9]

Compounds **2** reacted with LiPR₂ by the nucleophilic ring opening of the oxetane cycle to produce **3** after hydrolysis. After chromatographic workup, **3a** and **3c** were obtained as waxy solids, while **3b** formed an oil (Scheme 2).



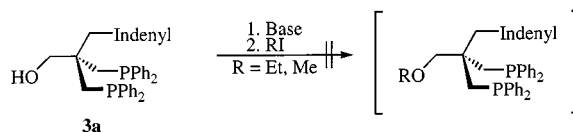
Scheme 2

The transformation of **2** into **3** occurred in yields between 62% and 73%. Analytical (Table 10) and spectroscopic data (Table 1) of **3** are in full agreement with the assigned structure. An almost complete assignment of the NMR peaks (except for those in the aromatic regions) is reported in Table 1.

Preliminary experiments into the coordination chemistry of **3** indicated that the presence of the OH group might cause problems: Deprotonation of **3a** by one equivalent of *n*BuLi and subsequent reaction with FeCl₂ or FeCl₂(PPh₃)₂^[10] resulted in insoluble, brown products of unknown composition. The same protocol, however, yields HOCH₂C(CH₂-η¹-PPh₂)₂(CH₂-η⁵-Cp)FeCl when the Cp analogue of **3a** is used.^[6] It appears that because the indenyl moiety is less acidic than the Cp moiety, deprotonation of the OH group of **3a** is a concomitant or even dominant reaction when **3a** is treated with *n*BuLi. The use of two equivalents of *n*BuLi did not improve the situation: Insoluble, brown products were again obtained. It was hoped to overcome this problem by protection of the hydroxy group as an ether derivative. It is known that transforming the CH₂OH groups of *neo*-pentane-based *tripod* ligands into ether functional groups is problematic.^[11] Special protocols have been developed in specific cases which overcome these problems, one of these special protocols being based on rigid temperature control under Williamson conditions.^[12]

Deprotonation of **3a** by *n*BuLi may be performed as a kind of titration, since a slight excess of *n*BuLi deprotonates the indenyl residue. The anion formed by deprotonation of the indenyl moiety is of an intense violet colour. The alkoxide which is obtained when **3a** is treated with one equivalent of *n*BuLi was allowed to react with methyl iodide or ethyl

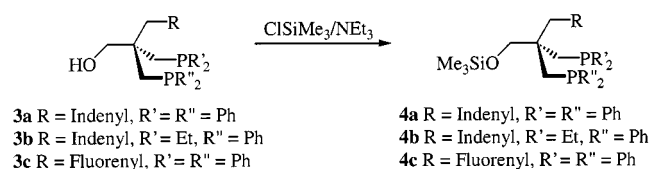
iodide in THF at temperatures from –15 °C up to 30 °C in different experiments (Scheme 3).



Scheme 3

The selective formation of just one product was not observed in any of the experiments. TLC analyses as well as mass spectrometric and NMR spectroscopic analyses revealed the formation of a mixture of many products in each case. A tentative explanation for this observation may be a proton-transfer equilibrium activating the indenyl part of the ligand with the resulting indenyl anion being far more reactive towards alkyl iodides than the alkoxide function. Alkyl substitution may therefore occur at the indenyl group.

This hypothesis was not further investigated, since it was found that the protection of the alcohol group of **3** is easily achieved by its reaction with trimethylchlorosilane, leading to the siloxy derivatives **4** (Scheme 4), which are obtained as colourless oils of high viscosity. The analytical and spectroscopic data of compounds **4** (Table 10 and Table 1) are in full agreement with the assigned structures.



Scheme 4

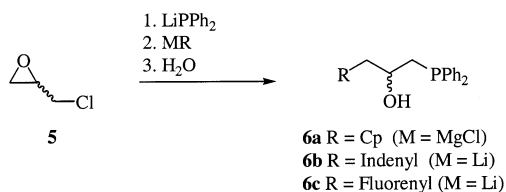
Starting from Epichlorohydrin

Epichlorohydrin (**5**) has been shown to be an efficient starting material for the synthesis of bidentate and tridentate chelate ligands.^[4] The tandem-type process of ring-opening and ring-closing steps occurring upon treating epichlorohydrin with phosphorus nucleophiles has been analysed in detail.^[4b,4c] An essential step in this synthetic approach is the nucleophilic opening of the oxirane ring by phosphide nucleophiles which has also been observed with some related oxirane starting materials.^[13] In the case of epichlorohydrin as the ligand precursor, this ring-opening step has also been shown to work with nitrogen and sulfur nucleophiles.^[4a] In view of this proven tolerance of the reaction, it appeared appealing to study the reactivity of **5** towards Cp nucleophiles.

It had already been shown by B. Rieger et al. that functionalised oxiranes may be attacked by Cp nucleophiles, with substitution at one of the oxirane carbon atoms and concomitant opening of the oxirane ring.^[14] With respect to the nucleophilic ring-opening reaction of oxiranes, the Cp nucleophiles show the same type of reactivity as phosphorus, nitrogen and sulfur nucleophiles. This type of reaction works as well with **5** as the starting compound. When **5** was treated with one equivalent of LiPPh₂, attack occurred at the unsubstituted oxirane carbon atom. The phos-

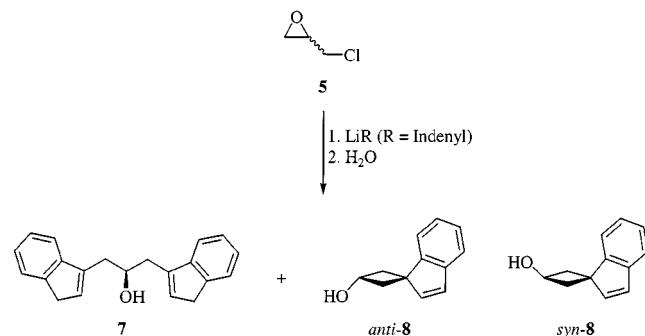
phane-substituted alkoxide resulting from this reaction may be characterised as an intermediate at low temperatures.^[4b,4c] At higher temperatures, the alkoxide oxygen atom attacks the CH₂Cl functional group with the formation of an oxirane, which may then be further attacked by nucleophiles at its unsubstituted carbon atom.^[4]

This sequence of steps, when performed with CpMgCl as the second nucleophile, led to the formation of **6a** in which a Cp unit and a PPh₂ unit are connected by a 2-hydroxy-1,3-propanediyl chain (Scheme 5). Compound **6a** was obtained as a mixture of two double-bond isomers (Table 2, ¹³C NMR). Its formation was always accompanied by the formation of some 1,3-bis(diphenylphosphanyl)-2-propanol, even when lower than stoichiometric quantities of LiPPh₂ were used. This by-product could not be separated from **6a** such that on first inspection, C,H analysis (Table 10) appeared to be inconsistent with the given formula. The relative content of this by-product was judged from the ¹H NMR spectrum of **6a** where the methine proton (at the 2-position of the C₃ chain) at the hydroxy-substituted carbon atom resonates at $\delta = 3.97$ (Table 2) while the HOCH(CH₂PPh₂)₂ proton gives rise to a signal at $\delta = 3.73$.^[4b,4c] Chromatographic separation of the products was not possible. It was, however, possible to obtain an analytically pure derivative of **6a** (**9a**, see below). When LiInd or LiFlu were used as the nucleophiles in the second preparation step, minor quantities of the corresponding diphosphanes were also obtained, but could be separated by chromatography such that **6b/6c** were obtained as analytically pure substances. Compounds **6a** and **6b** are colourless oils, and **6c** is a colourless solid. The composition of **6** is evident from microanalytical and mass spectrometric data (Table 10). The structure is unequivocally clear from their NMR spectra (Table 2).



Scheme 5

The sequence in which the nucleophiles are added to **5** is important. It had already been observed that spiro cyclisation may occur when an electrophilically activating group



Scheme 6

is present at the 4-position relative to a Cp carbon atom.^[2a] This type of reaction corresponds to the dominant reaction pathway when **5** is treated with Cp nucleophiles and this is apparent from the reaction of **5** with LiInd. When **5** was treated with five equivalents of LiInd, the disubstitution product **7** was obtained in only 4% yield while the spiro derivatives *syn*-**8**/*anti*-**8** were formed in 40% overall yield (Scheme 6).

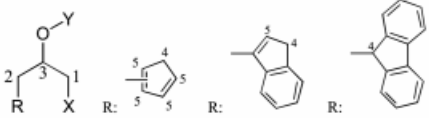
The assignment of *syn* and *anti* configurations to the two components of the product mixture followed the arguments explicitly described for closely analogous cases which were observed during indenyl substitution of *neo*-pentane-derived *tripod* ligands and was based on ¹H NMR spectroscopic data (Table 3).^[2a]

The isomers of **8** might in principle be separated by crystallisation as is demonstrated by the fact that upon crystallisation, single crystals of *anti*-**8** suitable for X-ray analysis were obtained. The structure of *anti*-**8** is shown in Figure 1 together with the structure of **7** from which single crystals could also be grown. There is nothing peculiar about the molecular structure of *anti*-**8**. Distances and angles are in the normal ranges (Table 4).

While the molecular symmetry of *anti*-**8** is C_s (Figure 1), the molecules aggregate in space group P4₁ to form a chiral crystal. The hydrophilic and hydrophobic parts of the molecule are embedded in specific compartments of the crystal with the hydroxy groups forming an infinite hydrogen-bonded spiral around a 4₁ axis of the P4₁-symmetric unit cell (Figure 2). The O...O distance between neighbouring oxygen atoms is only 265 pm. The position of the bridging hydrogen atoms has been determined by diffraction methods (H—O 83 pm, H...O 183 pm). The O...H—O angle is 174°. The hydrogen bonds are hence almost linear. The H—O...H angle is approximately 110°. A view of this interesting arrangement in the direction of the 4₁ axis is shown in Figure 2, giving an impression of the infinite hydrophilic channels along the crystal.

The structure of **7** (Figure 1) shows no peculiarities in the bond lengths and angles (Table 5). The position of the indenyl substituents is such that they are as far apart as possible with respect to the three-carbon linker between them. This type of orientation of indenyl and fluorenyl substituents linked by a three-carbon chain had already been observed for *tripod* ligands containing these groups.^[2a] The solid-state structure is again an interesting one. As already observed for *anti*-**8**, hydrophobic and hydrophilic compartments are well separated in the crystal. Compound **7** crystallises in the achiral space group P2₁/n. The hydroxy groups form hydrogen-bonded zigzag chains around the 2₁ axes of the unit cell. The O...O distances between the hydrogen-bonded oxygen atoms is only 274 pm. The H—O...H angle is 129°, the O—H distances were found to be 92 pm and 183 pm, with the O—H...O group being almost linear (168°).

It has been found that the transformation of enantiomerically pure epichlorohydrin into its disubstituted products HOCH(CH₂PR₂)(CH₂PR'₂) follows a completely enantioselective pathway.^[4] In order to find out if enantioselectiv-

Table 2. NMR spectroscopic data of compounds **6–7**, **9–12**^[a]


No.	R ^[b] X ^[b] Y ^[b]	1 ^[c] CH _{2a,b} [2H]	2 ^[c] CH _{2a,b} [2H]	3 ^[c] CH [1H]	4 ^[c] -CH _n - (n = 1–2)	5 ^[c] -CH=	CH aromatic	X	Y
6a	Cp PPh ₂ H	2.41 (m) 37.2, 37.4 (2d) ¹ J _{CP} = 13.0 Hz	2.75 (m) 39.4, 40.3 (2d) ² J _{CP} = 8.1 Hz	3.97 (m) 69.1, 69.7 (2d) ² J _{CP} = 16.2 Hz	2.92, 3.02 (2m) [2H] 42.0, 44.3 (2s)	6.17–6.50 (m) [3H]	7.35–7.55 (m) [10H] 128.8–146.3 {–24.6 (s)}	— {–24.6 (s)}	2.21 (bs) [1H] — —
6b	Indenyl PPh ₂ H	2.59 (d) ³ J _{HH} = 6.6 Hz 37.6 (d) ¹ J _{CP} = 13.4 Hz	2.95, 3.13 (2dd) ² J _{HH} = 14.3 Hz ³ J _{HH} = 7.9, 3.0 Hz 37.6 (d) ³ J _{CP} = 8.1 Hz	4.27 (m) 68.5 (d) ² J _{CP} = 16.6 Hz	3.45 (bs) [2H] 38.5 (s)	6.41 (s) [1H]	7.30–7.65 (m) [14H] 119.8–145.5 {–24.5 (s)}	— {–24.5 (s)}	2.53 (bs) [1H] — —
6c	Fluorenyl PPh ₂ H	2.32 (m) 38.8 (d) ¹ J _{CP} = 12.8 Hz	2.22, 2.45 (2m) [3H] 42.6 (d) ² J _{CP} = 7.8 Hz	4.05 (m) 68.1 (d) ² J _{CP} = 14.9 Hz	4.30 (m) [1H] 45.2 (s)	— —	7.30–7.88 (m) [18H] 120.4–147.8 {–25.6 (s)}	— {–25.6 (s)}	2.22 (m) [2H] — —
7	Indenyl Indenyl H	3.02 (m) 36.4 (s)	— —	4.52 (m) 69.2 (s)	3.52 (s) [4H] 38.5 (s)	6.53 (s) [2H]	7.30–7.65 (m) [8H] 119.7–145.7	— —	2.24 (s) [1H] —
9a	Cp PPh ₂ TMS	2.44 (pt) ³ J _{HH} = 5.8 Hz 37.7, 37.8 (2d) ¹ J _{CP} = 14.2 Hz	2.82 (m) 39.6, 40.3 (2d) ² J _{CP} = 8.4 Hz	4.05 (m) 71.1, 71.6 (2d) ² J _{CP} = 17.6 Hz	3.00 (m) [2H] 41.8, 44.9 (2s)	6.16–6.54 (m) [3H]	7.36–7.56 (m) [10H] 128.7–145.9 {–23.2 (s)}	— {–23.2 (s)}	0.08 (s) [9H] 0.7 (s) —
9b	Indenyl PPh ₂ TMS	2.50 (m) 38.3 (d) ¹ J _{CP} = 14.4 Hz	2.93, 3.14 (2dd) ² J _{HH} = 14.1 Hz ³ J _{HH} = 7.0, 4.5 Hz 37.7 (d) ³ J _{CP} = 8.6 Hz	4.24 (m) 70.3 (d) ² J _{CP} = 18.1 Hz	3.40 (s) [1H] 38.3 (s)	6.35 (s) [1H]	7.28–7.59 (m) [14H] 119.8–145.9 {–23.5 (s)}	— {–23.5 (s)}	–0.01 (s) [9H] 0.6 (s) —
12a	Cp PPh ₂ PPh ₂	2.47, 2.68 (2dd) ² J _{HH} = 13.9 Hz ³ J _{HH} = 7.2, 6.1 Hz 36.2 (dd) ¹ J _{CP} = 15.3 Hz ³ J _{CP} = 14.4 Hz	2.80–3.00 (m) 37.9, 38.7 (2dd) ³ J _{CP} = 5.5, 8.3 Hz	4.31 (m) 79.0 (m)	3.00 (m) [2H] 41.8, 44.5 (2s)	6.10–6.49 (m) [3H]	7.37–7.58 (m) [20H] 128.5–146.2 {–24.7, –24.8 (2d)} { ⁴ J _{PP} = 5.9 Hz}	— {106.7, 106.8 (2d)} { ⁴ J _{PP} = 5.9 Hz}	— — —
12b	Indenyl PPh ₂ PPh ₂	2.55, 2.71 (2dd) ² J _{HH} = 13.9 Hz ³ J _{HH} = 6.7, 5.9 Hz 36.8 (dd) ¹ J _{CP} = 15.6 Hz ³ J _{CP} = 5.5 Hz	3.17 (d) ³ J _{HH} = 6.2 Hz 36.4 (dd) ³ J _{CP} = 8.7, 6.0 Hz	4.52 (m) 78.2 (dd) ² J _{CP} = 20.1, 17.0 Hz	3.22 (s) [2H] 38.4 (s)	6.20 (s) [1H]	7.24–7.58 (m) [24H] 119.9–144.5 {–24.9 (d)} { ⁴ J _{PP} = 5.6 Hz}	— {107.0 (d)} { ⁴ J _{PP} = 5.6 Hz}	— — —
12c	Fluorenyl PPh ₂ PPh ₂	2.42, 2.79 (2m) 37.5 (dd) ¹ J _{CP} = 15.6 Hz ³ J _{CP} = 5.9 Hz	— 42.2 (m)	4.54 (m) 77.4 (dd) ² J _{CP} = 15.7, 18.8 Hz	4.25 (m) [1H] 44.7 (s)	— —	7.28–7.89 (m) [28H] 120.3–148.1 {–25.8 (d)} { ⁴ J _{PP} = 5.9 Hz}	— {105.8 (d)} { ⁴ J _{PP} = 5.9 Hz}	— — —
10	Cp PPh ₂ BH ₃ H	2.4–3.0 (m) [7H] 33.72, 33.77 (2d) ¹ J _{CP} = 36.3 Hz	— 39.4, 40.3 (2d) ³ J _{CP} = 11.4 Hz	4.18 (m) 67.5 (d) ² J _{CP} = 24.1 Hz	2.4–3.0 (m) [7H] 42.0, 44.2 (2s)	6.12–6.49 (m) [3H]	7.43–7.77 (m) [10H] 0.4–1.9 (bs) [3H] {9.7, 10.5 (2s)}	— — —	2.4–3.0 (m) [7H] —
11	Cp PPh ₂ BH ₃ Ms	2.58 (m) [4H] 31.3, 32.0 (2d) ¹ J _{CP} = 13.1, 12.7 Hz	— 36.9, 37.9 ³ J _{CP} = 5.1, 5.5 Hz	5.19 (m) 79.1, 79.2 (2d) ² J _{CP} = 4.5, 5.0 Hz	2.97 (m) [5H] 42.0, 44.4 (2s)	6.18–6.47 (m) [3H]	7.46–7.86 (m) [10] 0.7–1.9 (bs) [3H] {10.3 (bs)}	— — —	2.97 (m) [5H] — 38.3, 38.6 (2s)

^[a] For ease of comparison, the sequence of entries in this table does not follow the numbering scheme; sequence of entries for each compound: ¹H NMR, ¹³C{¹H} NMR, ³¹P{¹H} NMR spectroscopic data are embedded in curly brackets; solvent: CDCl₃; CH_{2a,b} designates CH₂ groups whose protons may be diastereotopic depending on the symmetry of the compound; lines adjacent to individual column entries indicate that signals referring to the columns to which these lines extend are within the range given in each case or are mapped to one and the same signal. — ^[b] This column refers to the composition of the individual compounds with reference to the graphical illustration (Footnote^[c]). — ^[c] Designators of the individual groups as used in the header of the table: see graphics on top of the table.

ity could also be achieved when Cp nucleophiles were used in the second step of the transformation, the one-pot synthesis of **6b** was performed with enantiomerically pure *S*-(+)-**5** as well as with *R*-(–)-**5** (Scheme 7).

Compound *R*-(–)-**6b** was obtained from *S*-(+)-**5** in a yield of 42%, showing a specific rotation of $[\alpha]_{\text{D}}^{20} = -18.73 \pm 0.53$. Compound *S*-(+)-**6b** was obtained from *R*-(–)-**5** in the same yield. The optical rotation for this product was

	No.	1 ^[b] CH [1H]	2 ^[b] CH _{2a,b} [4H]	3 ^[b] C _q	4 ^[b] -CH= [1H]	5 ^[b] -CH= [1H]	CH aromatic [4H]	6 ^[b] OH [1H]
¹ H-NMR	<i>syn</i> - 8	4.77 (dt) ³ J _{HH} = 15.1, 7.4 Hz	2.75 (m)	—	6.73, 6.82 (2d) ³ J _{HH} = 5.4 Hz	—	7.30–7.73 (m)	3.57 (bs)
	<i>anti</i> - 8	5.02 (dt) ³ J _{HH} = 14.6, 7.3 Hz	2.75 (m)	—	6.56, 6.78 (2d) ³ J _{HH} = 5.4 Hz	—	7.30–7.73 (m)	3.57 (bs)
¹³ C{ ¹ H}-NMR	<i>syn</i> - 8	62.8 (s)	41.3 (s)	46.8 (s)	—	—	121.5–152.1	—
	<i>anti</i> - 8	63.8 (s)	41.1 (s)	47.6 (s)	—	—	121.5–152.1	—

^[a] Solvent CDCl₃. – ^[b] Designators of the individual groups as used in the header of the table: see graphics on top of the table.

[a]

C1—O	141.5(3)	O—C1—C3	120.0(3)
C1—C2	152.9(4)	O—C1—C2	118.7(2)
C1—C3	154.2(4)	C5—C4—C8	101.7(2)
C2—C4	155.5(4)	C3—C4—C8	115.5(2)
C3—C4	156.6(4)	C2—C4—C8	116.2(2)
C4—C5	151.3(3)	C3—C4—C5	119.3(2)
C5—C6	133.3(4)	C2—C4—C5	117.9(2)
C6—C7	146.8(4)	O—C1—C2—C4	143.9(3)
C7—C8	140.3(4)	O—C1—C3—C4	−142.7(3)
C4—C8	151.2(4)	C1—C3—C4—C2	19.5(2)
C _{ar} —C _{ar}	138.1(4)–	C2—C1—C3—C4	−19.8(2)
	139.3(4)	C1—C3—C4—C8	−98.3(2)
C1—C2—C4	89.0(2)	C1—C2—C4—C8	97.5(3)
C1—C3—C4	88.1(2)	C1—C3—C4—C5	140.0(3)
C2—C1—C3	88.9(2)	C1—C2—C4—C5	−141.5(3)
C2—C4—C3	87.1(2)		

^[a] The numbering scheme used refers to the scheme shown in Figure 1; it is different from the scheme used to label individual atoms in the deposited data; C_{ar}–C_{ar} designates the distances within the anellated cycles excluding C7–C8 which is given explicitly.

$[\alpha]_{\text{D}}^{20} = 17.28 \pm 0.48$. The optical rotations are thus opposite in sign but equal in size (within the limits of error). While this is no proof for complete enantioselectivity, it agrees with the observations that the reaction is completely enantioselective when using phosphorus nucleophiles.^[4] It also agrees with the results of similar reactions with other types of oxiranes in which complete enantioselectivity is observed.^[14]

Since the hydroxy groups in **6** might complicate the coordination of these ligands, protection of these groups was considered to be important. As already experienced with **3**, ether formation under Williamson conditions was not successful with **6**; only inseparable mixtures of compounds were obtained. In contrast, protection with chlorotrimethyl-

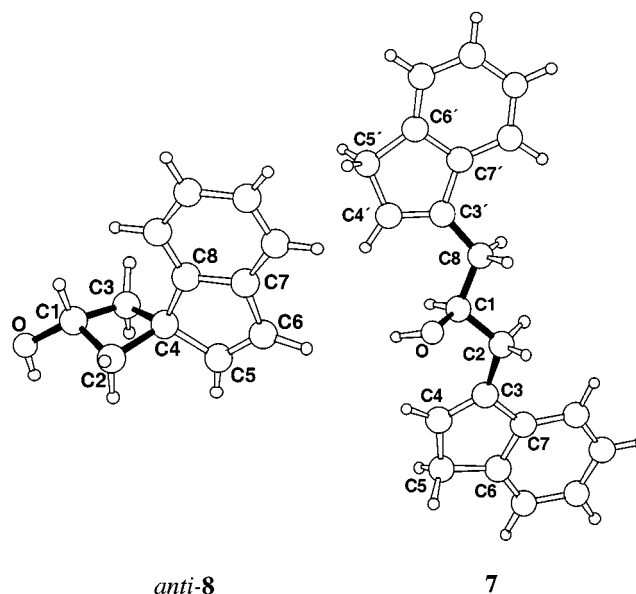


Figure 1. Structures of **7** and *anti*-**8**

silane did not cause any problems and the siloxy derivatives **9** were prepared (Scheme 8).

Silylation of **6a** proceeded in close to quantitative yields and is also a good method to purify **6a**, since **9a** is easily separated from $\text{Me}_3\text{SiOCH}(\text{CH}_2\text{PPh}_2)_2$ by chromatography. Both compounds **9** were fully characterised by their analytical and spectroscopic data (Table 2 and Table 10).

In order to activate the hydroxy group of **6** it was not protected but instead the mesylate **11** was synthesised. For this purpose, the phosphane group had to be protected. Addition of $\text{BH}_3 \cdot \text{THF}$ led to the formation of **10** (Scheme 9).

Compound **10** was obtained as an analytically pure, colourless oil after chromatographic workup (Table 10). In contrast to the other Cp derivatives containing phosphorus

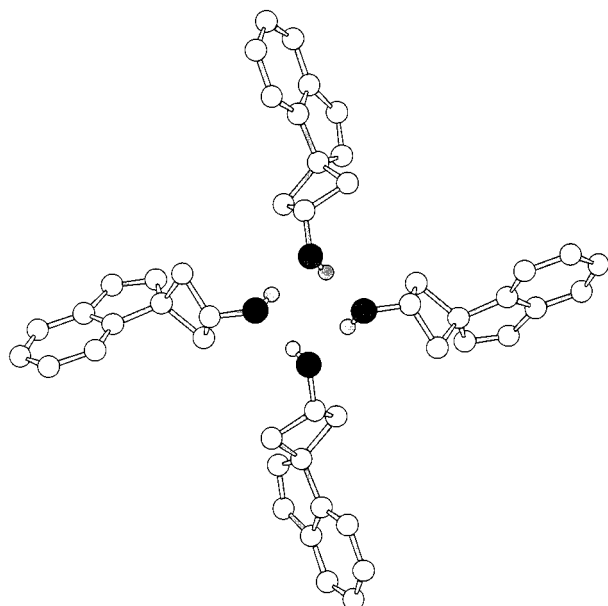


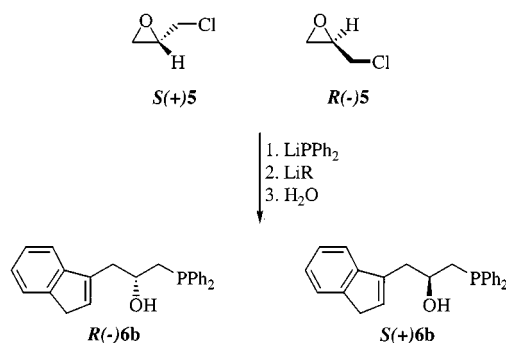
Figure 2. The hydrogen-bonded spiral formed by *anti*-8 in the crystal in a projection along its 4₁ axis

Table 5. Selected bond lengths [pm], bond angles [°], and torsion angles [°] of **7**

[a]

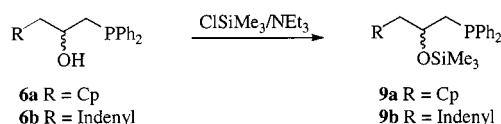
C1–O	144.3(2)	C3–C7	147.6(3)
C1–C2	152.5(3)	C3'–C7'	147.9(3)
C1–C8	152.3(3)	C _{ar} –C _{ar}	138.5(3)–
C2–C3	150.0(0)		139.2(3)
C8–C3'	149.3(3)	O–C1–C2	117.2(2)
C3–C4	134.5(3)	O–C1–C8	109.9(2)
C3'–C4'	135.0(3)	C2–C1–C8	110.2(2)
C4–C5	150.2(3)	C1–C2–C3	117.2(2)
C4'–C5'	150.1(3)	C1–C8–C3'	117.2(2)
C5–C6	150.6(3)	O–C1–C2–C3	71.5(2)
C5'–C6'	150.3(3)	O–C1–C8–C3'	–65.0(2)
C6–C7	140.3(3)	C1–C2–C3–C4	–15.2(3)
C6'–C7'	140.7(3)	C1–C8–C3'–C4'	4.9(3)

[a] The numbering scheme used refers to the scheme shown in Figure 1; it is different from the scheme used to label individual atoms in the deposited data; C_{ar}–C_{ar} designates the distances within the annellated cycles excluding C6–C7 and C6'–C7' which are given explicitly.

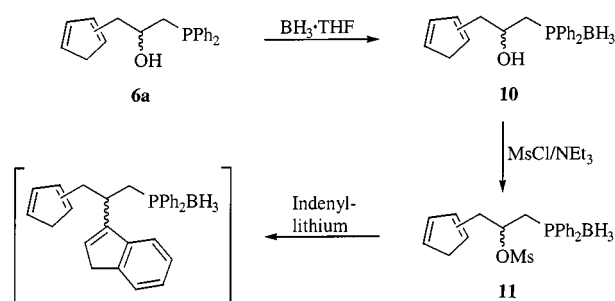


Scheme 7

donor groups described in this paper, the double bond isomers of **10** are resolved in its ³¹P NMR spectrum (Table 2). This is consistent with earlier findings reported for some



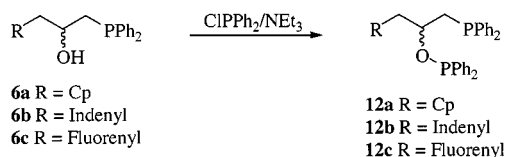
Scheme 8



Scheme 9

ligands containing Cp and PPh₂BH₃ substituents.^[2b] Mesylation of **10** by standard methods led to **11**, which was obtained as a colourless oil after chromatography. Analytical and spectroscopic data (Table 10 and Table 2) confirmed its identity. To test the reactivity of the mesylate functional group in this compound, **11** was treated with two equivalents of indenyllithium. Hydrolysis and chromatographic workup gave only a mixture of products, among which the expected product was clearly present as shown by mass spectrometry (prominent signal at *m/z* = 420 [*M*⁺]). Further purification was not possible.

Compounds **6** are also suitable starting materials for the synthesis of tripodal ligands. Their reaction with ClPPh₂ produced **12** containing one CH₂Cp[#], one CH₂PPh₂ and one OPPh₂ group. Compounds **12a** and **12b** were obtained as colourless oils while **12c** was a waxy solid (Scheme 10).

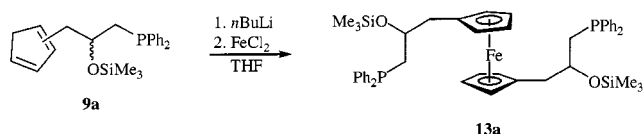


Scheme 10

Mass spectra, elemental analyses and NMR spectra are consistent with the given structures (Table 10 and Table 2). The double-bond isomers of **12a** give rise to separate peaks in the ³¹P NMR spectrum (Table 2). The impurity of **6a** [HOCH(CH₂PPh₂)₂, see above] was transformed into its OPPh₂ derivative.^[4] This derivative was present as an impurity in **12a** and could not be separated by chromatography (but compare **9a**, see above). Its elemental composition was determined by HRMS while **12b** and **12c** gave highly satisfying C,H analyses (Table 10). The NMR spectroscopic data (Table 2) were consistent with the given formulas; **12b** and **12c** also showed two separate peaks for their double-bond isomers in the ³¹P NMR spectra (Table 2).

Coordination Chemistry

Tripodal ligands $\text{RCH}_2\text{C}(\text{CH}_2\text{PR}'_2)(\text{CH}_2\text{PR}_2'')(\text{CH}_2\text{Cp})$ have been shown to form *tripod* metal templates $\text{RCH}_2\text{C}(\text{CH}_2\text{-}\eta^1\text{-PR}'_2)(\text{CH}_2\text{-}\eta^1\text{-PR}_2'')(\text{CH}_2\text{-}\eta^5\text{-Cp})\text{M}$ with iron, manganese, molybdenum and ruthenium.^[2,3,6,15] The procedures leading to manganese and molybdenum derivatives are complicated multi-step reactions and therefore were not suitable to test the coordination capabilities of Cp-containing *tripod* ligands.^[2b,3a] In contrast, derivatives of the type $\text{RCH}_2\text{C}(\text{CH}_2\text{-}\eta^1\text{-PR}'_2)(\text{CH}_2\text{-}\eta^1\text{-PR}_2'')(\text{CH}_2\text{-}\eta^5\text{-Cp})\text{MCl}$ have been obtained for $\text{M} = \text{Fe}$ and Ru by convenient one-step procedures.^[2a,3b,6,15] The different classes of ligands described in this paper were therefore initially tested for their reactions with FeCl_2 or $\text{FeCl}_2(\text{PPh}_3)_2$.^[10] Compounds **4** did, after deprotonation with $n\text{BuLi}$, react with these reagents to yield deep-brown THF solutions from which no pure compounds could be isolated. In contrast, compounds **9** reacted with $\text{FeCl}_2(\text{PPh}_3)_2$ ^[10] under similar conditions to yield the ferrocene derivatives **13** instead of the corresponding $\text{CpLFePPh}_3\text{Cl}$ compounds. These ferrocene derivatives were obtained in good yields when FeCl_2 was used as the starting material (Scheme 11).



Scheme 11

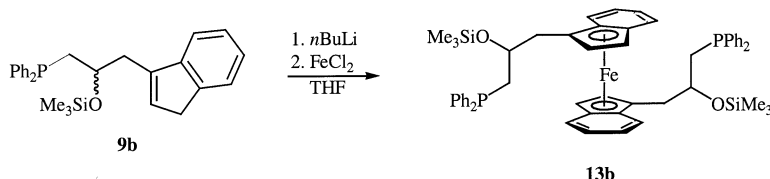
Compound **13a** was obtained from **9a** as a yellow, waxy material in analytically pure form (Table 11). With two stereogenic centres, **13a** must exist as a mixture of *meso* and *racemic* forms. The interaction of the chiral groups is, however, too small to make this differentiation recognisable in its NMR spectra. Only one set of signals was observed for each group (see Experimental Section). One sharp ^{31}P NMR resonance is observed at $\delta = -23.6$. The Cp protons give rise to one unresolved signal at $\delta = 4.01$. Regarding the diastereotopic methylene protons, the pair at the CH_2Cp group gives rise to a well-resolved pattern at $\delta = 2.77$ with $^2J_{\text{HH}} = 14.0$ Hz and $^3J_{\text{HH}} = 6.0$ Hz (see Experimental Section) while those of the CH_2PPh_2 group appear as an unresolved multiplet at $\delta = 2.26$ (see Experimental Section). The ^{13}C NMR spectra show well-resolved peaks for the individual types of carbon atoms and allowed for the complete assignment of the Cp carbon atoms as well as of the carbon atoms of the side chains (see Experimen-

tal Section). As is characteristic for ferrocene and its derivatives **13a** shows a reversible oxidation in its cyclovoltammogram. The electronic influence of the side chains in **13a** is small, since oxidation occurs at $E_{1/2} = 325$ mV (vs. SCE), while ferrocene – under the same conditions – is oxidised at $E_{1/2} = 367$ mV.

The presence of free phosphane donors in **13a** is also apparent from its ^{31}P NMR signal at $\delta = -23.6$ (see Experimental Section). Additional evidence came from the reaction of **13a** with $\text{Cr}(\text{CO})_5\text{THF}$ which resulted in a yellow, waxy substance. The mass spectrum of this yellow material shows a peak at $m/z = 1198$ [M^+ , **13b**·2 $\text{Cr}(\text{CO})_5$], which by consecutive loss of CO groups and one Cr atom, leads to a prominent signal at $m/z = 866$. Reaction of **9b** with FeCl_2 gave **13b** as a dark red, viscous oil (Scheme 12).

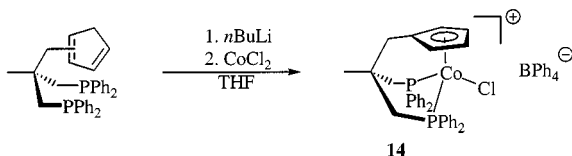
The number of stereoisomers is increased by a factor of two with respect to the number of isomers of **13a**, the reason being the loss of symmetry on going from the monosubstituted Cp ligand in **13a** to the monosubstituted indenyl ligand in **13b**. Nevertheless, only one sharp ^{31}P NMR signal is observed for **13b** at $\delta = -23.5$. The ^1H NMR spectrum of **13b**, on the other hand, clearly shows two different sets of signals with an intensity ratio of approximately 1:1. Thus, two signals are observed for the TMS protons, one at $\delta = -0.25$ and the other at $\delta = -0.20$. Two well-separated signals are also observed for the protons at the 3-position of the indenyl ligands, one at $\delta = 4.48$ and the other one at $\delta = 4.36$. The signals relating to the other protons partly overlap. COSY experiments,^[16] nevertheless, allowed for their unambiguous assignment. It followed that there are two classes of isomers of **13b** which are discernible by ^1H NMR spectroscopic data. ^{13}C NMR spectroscopic data are in agreement with these findings (see Experimental Section). Since it had been shown with **13a** as the example that the chirality of the substituents does not lead to separate signals for the corresponding diastereomers, the two classes of isomers observed for **13b** must be due to the two sets of diastereomers which result by formally adding the R–IndFe entity to either of the two sides of the second R–Ind ligand. Compound **13b** shows a reversible oxidation, as one would expect for a ferrocene derivative with $E_{1/2} = 106$ mV (vs. SCE). It is more readily oxidised than ferrocene which shows its oxidation peak at 470 mV in the same experiment.

The reactions of **4** and **9** with FeCl_2 and $\text{FeCl}_2(\text{PPh}_3)_2$ ^[10] did not produce compounds in which the Cp-type donor and the phosphorus donors bind in a chelate mode. To test whether CoCl_2 might be an appropriate precursor for the formation of such chelate compounds, the prototype ligand



Scheme 12

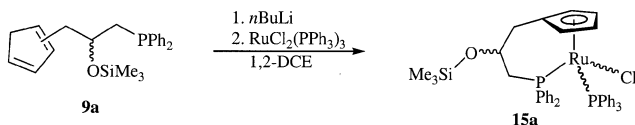
$\text{CH}_3\text{C}(\text{CH}_2\text{PPh}_2)_2(\text{CH}_2\text{Cp})^{[2b]}$ was treated with $\text{CoCl}_2 \cdot \text{THF}$ (Scheme 13).



Scheme 13

From the dark brown reaction mixture, the violet chelate compound was separated by chromatography and isolated as its analytically pure BPh_4 salt **14**. The ^{31}P NMR resonance of **14** occurs at $\delta = 25.4$. The ^1H NMR spectrum, as well as the ^{13}C NMR spectrum, confirm the assigned structure (see Experimental Section). The isolation of **14** showed that CoCl_2 might be a suitable starting material to obtain the desired chelate compounds. Since the yield of **14** was lower than the yields of the corresponding iron compounds,^{[2a][3b,6]} $\text{RuCl}_2(\text{PPh}_3)_3$ was tested as an alternative precursor. It had been found that its reaction with $\text{CH}_3\text{C}(\text{CH}_2\text{PPh}_2)_2(\text{CH}_2\text{Cp})$ produces $\text{CH}_3\text{C}(\text{CH}_2\text{-}\eta^1\text{-PPh}_2)_2(\text{CH}_2\text{-}\eta^5\text{-Cp})\text{RuCl}$ in yields of up to 41% and it had also been observed that this compound, once formed, is quite stable.^[15] Thus, the coordination capabilities of the ligands **9** were tested once again with $\text{RuCl}_2(\text{PPh}_3)_3$ as the starting coordination compound.

When **9a** was deprotonated by $n\text{BuLi}$ in THF, a yellow, oily product remained after evaporation of the solvent. Addition of a solution of this residue in 1,2-dichloroethane to a solution of $\text{RuCl}_2(\text{PPh}_3)_3$ in 1,2-dichloroethane produced a slightly brown reaction mixture. Keeping this reaction mixture at 90°C for 1 h resulted in the formation of **15a** as a yellow crystalline powder in yields of 50% after chromatographic workup (Scheme 14, Table 11). The chirality at the siloxy-substituted carbon atom and the metal-centred chirality result in **15a** existing as two diastereomers, each comprising of an enantiomeric pair. The ^{31}P NMR spectrum of **15a** shows two well-resolved doublets of high intensity and two equally well-resolved doublets with about $1/10$ of the intensity of the two major doublets (Experimental Section). The assumption that these two patterns arise from two diastereomers present in a ratio of 10:1 was justified by the ^1H NMR spectrum of **15a**. Four well-separated signals are observed for the Cp protons of the major isomer. Two of the four Cp protons of the minor isomer give rise to well-separated signals, while the other two are hidden under the signals of the methine protons and of one of the Cp protons of the major isomer (see Experimental Section). The diastereomeric ratio, as inferred from the corresponding integrals, was 13:1.



Scheme 14

Diastereomeric discrimination has already been observed in the preparation of other similar compounds. B. Trost et al. have tested a series of chelate ligands which contain a Cp moiety covalently linked to a PPh_2 entity by a chiral spacer. When these ligands were used in the preparation of compounds of type **15a**, diastereomeric ratios of up to 5:1 were observed with $-(\text{CH}_2)_3-(\text{H})(\text{CH}_2\text{Ph})\text{C}-$ as the chiral linker, the stereogenic centre being bonded to the phosphorus atom.^[17] Single crystals of **15a** were obtained in about 80% yield by slow evaporation of the solvent from saturated $\text{CH}_2\text{Cl}_2/\text{PE}$ (boiling range $40-60^\circ\text{C}$) solutions.

X-ray analysis showed them to contain the racemate of **15a** with two independent molecules **15a** in the asymmetric unit of the centrosymmetric unit cell (Table 6 and Figure 3). The configuration at the stereogenic centres of the analysed diastereomer was *R,R* and *S,S*. Based on the high yield with which single crystals were obtained, it was assumed that the major isomer was the diastereomer contained in the crystal. The chelate cycle formed by C4, C3, C2, C1, P1 and Ru1 adopts an approximate chair conformation (Figure 3; Table 6, torsion angles). The OSiMe_3 group is in an equatorial position (Figure 3 and Table 6) of this cycle. The PPh_3 ligand occupies an axial position, with the Cl ligand lying in an equatorial position with respect to this idealised description (Figure 3 and Table 6). The coordination around the ruthenium centre (Figure 3) is similar to that observed in other derivatives of the type CpRuL_2Cl .^[15] The rotational position of the phenyl groups of the PPh_2 moiety of the chelate ligand corresponds to the generally observed position in *tripod* metal compounds $\text{H}_3\text{CC}(\text{CH}_2\text{-}\eta^1\text{-PPh}_2)_2(\text{CH}_2\text{-}\eta^5\text{-Cp})\text{RuCl}$.^[15] The phenyl groups of the PPh_3 ligand adopt the usual propeller-type arrangement (Figure 3). Bonding to the Cp ligand is symmetric, and all the $\text{Ru}-\text{C}^{\text{Cp}}$ distances are similar (Table 6). The Cp ligand is planar to within ± 1 pm. The carbon atom of the chelate chain which bonds to the Cp entity (Figure 3, C3) deviates from this plane by 16 pm (14 pm in the other independent molecule) in a direction opposite to the ruthenium centre.

Table 6. Selected bond lengths [pm], bond angles $^\circ$, and torsion angles $^\circ$ of **15a**

[a]			
Ru1–P1	228.3(2)/227.9(2)	C6–C7	142.6(9)/140.8(8)
Ru1–P2	231.1(2)/231.3(2)	C7–C8	144.1(9)/141.8(8)
Ru1–C4	219.1(6)/218.8(6)	P1–Ru1–P2	99.5(1)/98.5(1)
Ru1–C5	221.1(6)/223.3(6)	P1–Ru1–Z	119.1/119.8
Ru1–C6	222.6(6)/223.7(6)	P2–Ru1–Z	124.6/124.5
Ru1–C7	224.8(6)/222.0(6)	P1–Ru1–Cl1	95.1(1)/94.8(1)
Ru1–C8	218.3(6)/218.6(6)	P2–Ru1–Cl1	89.9(1)/91.4(1)
Ru1–Z	184.9/185.1	Z–Ru1–Cl1	121.4/120.7
Ru1–Cl1	244.4(2)/244.8(2)	C2–C1–P1–Ru1	–58.6(5)/53.1(5)
C3–C4	151.4(9)/150.1(8)	C1–C2–C3–C4	–63.2(7)/59.1(7)
C4–C5	143.8(9)/145.2(9)	C2–C3–C4–Ru1	46.1(8)/–45.3(7)
C4–C8	142.1(9)/143.1(8)	C3–C4–C5–C6	173.1(6)/173.3(6)
C5–C6	140.9(9)/140.9(9)	C3–C4–C8–C7	171.7(5)/–173.1(6)

[a] Atom identifiers refer to Figure 3; Z designates the centre of the Cp ligand. There are two independent molecules **15a** in the crystal; the data referring to the second molecule are given following the slash in each case.

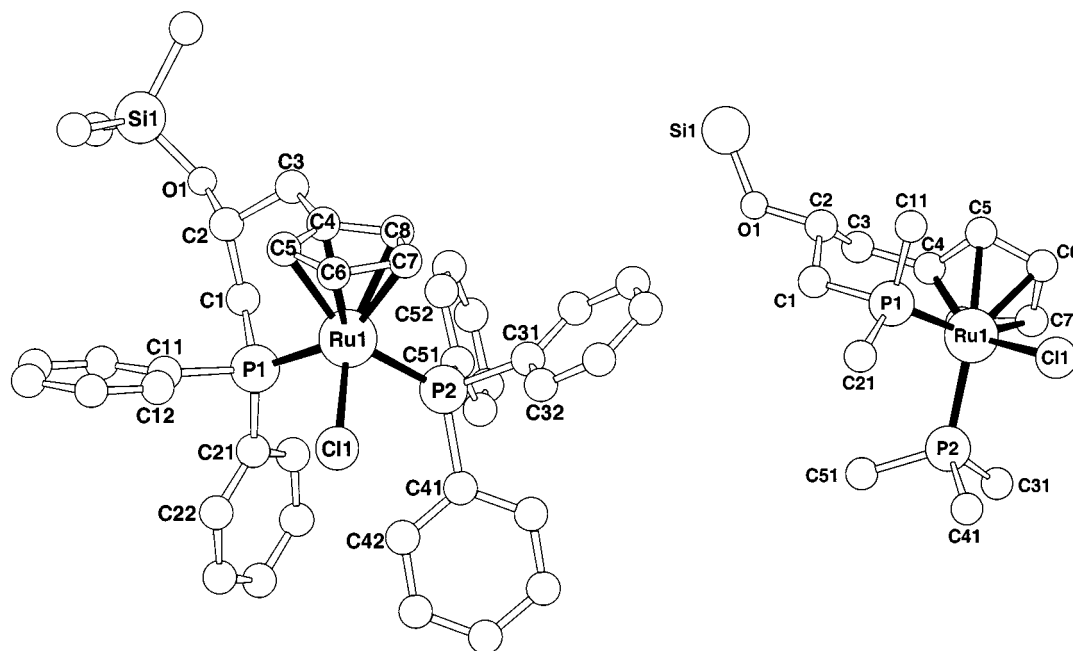


Figure 3. Structure of **15a**; left-hand side: general view and labelling scheme; right-hand side: view showing the chair conformation of the chelate cycle

The structure of the second diastereomer, which is formed in only 7% relative to the major isomer, must correspond to the one in which the positions of the PPh_3 and the Cl ligands are exchanged. Inspection of Figure 3 shows that steric crowding should increase by this exchange.

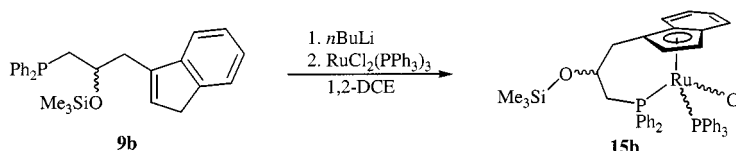
The number of possible isomers (four in the case of **15a**) occurring as two diastereomeric pairs will be increased by a factor of two when **9b** acts as a ligand in **15b**, due to the additional chirality introduced by anellating the Cp moiety.

The reaction of **9b** with $\text{RuCl}_2(\text{PPh}_3)_3$ under similar conditions used in the preparation of **15a** might thus, in principle, lead to the formation of four diastereomeric forms of **15b** (Scheme 15), each of them comprising of an enantiomeric pair, and the results of such a reaction might therefore be difficult to analyse. On the other hand, the diastereomeric discrimination already observed in the formation of **15a** might even be enhanced by the additional steric congestion introduced by the anellated benzene ring in the indenyl derivative compared to the Cp derivative. This is, in fact, found in the experimental results. Only two sharp and well-resolved doublets are observed for **15b** in its ^{31}P NMR spectrum. The ^1H NMR spectrum shows sets of signals which can unequivocally be assigned to only one diastereomer, with no indication of any contamination by other diastereomers. The signals for the methylene and the methine protons of the chelate cycle as well as the resonances of the two Cp protons are observed in the range between $\delta = 2.4$

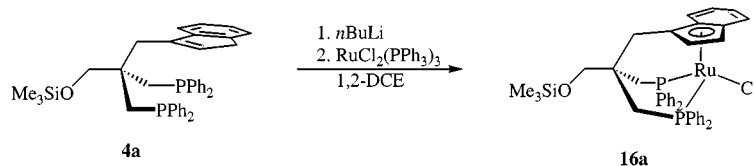
and $\delta = 4.5$ (see Experimental Section). Assignment of the individual resonances was possible by analysis of the individual coupling constants, as well as by ^{31}P decoupling. In the ^{13}C NMR spectrum of **15b**, the corresponding resonances can unambiguously be assigned. The *ipso*-carbon atoms of the indenyl moiety were also identified by their corresponding signals. No attempt was made to assign the signals in the arene region.

All these NMR spectra show that only one diastereomer was formed by the reaction of **9b** with $\text{RuCl}_2(\text{PPh}_3)_3$. Based on the known structure of **15a**, it appears that anellation of the Cp moiety at the side of the chelate chain would lead to less steric crowding than anellation at the PPh_3 side. Replacing the Cp moiety in **15a** by the indenyl group, as in **15b**, resulted in an increase in diastereomeric differentiation and **15b** was formed exclusively in one diastereomeric form.

With *tripod* ligands such as **4b**, which have a stereogenic carbon centre by virtue of their two different phosphorus donors, diastereomeric differentiation might also be expected in their tripodal-coordinated derivatives. In order to test the coordination capabilities of **4**, the achiral ligand **4a** was deprotonated with *n*BuLi and treated with $\text{RuCl}_2(\text{PPh}_3)_3$. Chromatographic workup led to **16a** (Scheme 16). The yield of **16a** (42%) (Table 11) appeared sufficient to also test the less easily accessible ligand **4b** in this type of reaction. A modest yield of 16% of **16b** was obtained (Table 11, Scheme 17).



Scheme 15

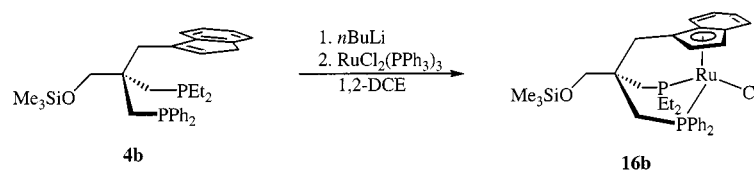


Scheme 16

Table 7. ^1H and $^{31}\text{P}\{^1\text{H}\}$ NMR spectroscopic data of compounds **16**

Atom ^{[a][b]}	16a	16b	Atom ^[b]	16a	16b	Atom ^[b]	16a	16b
H^{1a}	2.40 (dd) [1H] $^2J_{\text{HH}} = 15.5 \text{ Hz}$, $^2J_{\text{HP}} = 10.3 \text{ Hz}$	1.15 (m)	H¹¹	7.27 (m)	—	H⁴	4.66 (dd) [1H] $^3J_{\text{HH}} = 2.7 \text{ Hz}$	4.53 (dd) $^3J_{\text{HH}} = 2.5 \text{ Hz}$
H^{1b}	2.55 (dd) [1H] $^2J_{\text{HH}} = 15.5 \text{ Hz}$, $^2J_{\text{HP}} = 9.4 \text{ Hz}$	1.55 (m)	H²¹	7.33 (m)	—	H⁵	$J_{\text{HP}} = 7.2 \text{ Hz}$	$J_{\text{HP}} = 8.4 \text{ Hz}$
H^{2a}	2.91 (dd) [1H] $^2J_{\text{HH}} = 15.4 \text{ Hz}$, $^2J_{\text{HP}} = 10.7 \text{ Hz}$	2.98 (dd) [1H] $^2J_{\text{HH}} = 15.1 \text{ Hz}$, $^2J_{\text{HP}} = 11.4 \text{ Hz}$	H⁴¹	7.36 (m)	7.80 (m)	H⁶	5.73 (dd) [1H] $^3J_{\text{HH}} = 2.7 \text{ Hz}$	5.59 (m) $^3J_{\text{HH}} = 2.5 \text{ Hz}$
H^{2b}	2.01 (m) [1H]	1.75 (m)	H^{11a}	8.06 (dd) $^3J_{\text{HH}} = 6.6 \text{ Hz}$, $^3J_{\text{HP}} = 7.8 \text{ Hz}$	8.10 (dd) $^3J_{\text{HH}} = 6.6 \text{ Hz}$, $^3J_{\text{HP}} = 8.5 \text{ Hz}$	H⁷	$J_{\text{HP}} = 3.3 \text{ Hz}$	7.60 (d) [1H] $^3J_{\text{HH}} = 8.2 \text{ Hz}$
H^{3a}	2.06 (d) [1H] $^2J_{\text{HH}} = 14.4 \text{ Hz}$	1.92 (m)	H^{11b}	—	1.55 (m)	H⁸	7.04 (t) $^3J_{\text{HH}} = 7.3 \text{ Hz}$	7.58 (d) [1H] $^3J_{\text{HH}} = 7.4 \text{ Hz}$
H^{3b}	1.84 (d) [1H] $^2J_{\text{HH}} = 14.4 \text{ Hz}$	1.92 (m)	H¹²	—	0.38 (m)	H⁹	6.23 (t) $^3J_{\text{HH}} = 7.6 \text{ Hz}$	7.26 (m)
CH₂O	3.85 (br. s) [2H]	3.63 (br. s) [2H]	H^{21a}	—	0.15 (m)	H⁹	6.07 (d) $^3J_{\text{HH}} = 8.2 \text{ Hz}$	7.58 (m)
SiCH₃	0.36 (s) [9H]	0.28 (s) [9H]	H^{21b}	—	1.15 (m)			7.21 (m)
P¹	30.4 (d) $^2J_{\text{PP}} = 80.2 \text{ Hz}$	33.8 (d) $^2J_{\text{PP}} = 77.1 \text{ Hz}$	H²²	—	0.65 (dt) $^3J_{\text{HH}} = 7.4 \text{ Hz}$, $^3J_{\text{HP}} = 7.2 \text{ Hz}$			
P²	54.0 (d) $^2J_{\text{PP}} = 80.2 \text{ Hz}$	56.3 (d) $^2J_{\text{PP}} = 77.1 \text{ Hz}$						

[a] Solvent CDCl_3 . — [b] For designation of the atoms refer to Figure 6 (**16a**) and Figure 9 (**16b**).



Scheme 17

Both compounds **16** were obtained as red, microcrystalline powders. Two sharp doublets are observed in the ^{31}P NMR spectrum of **16a** ($\delta = 30.4, 54.0$, $^2J_{\text{PP}} = 80.2 \text{ Hz}$, Table), as is expected owing to its lack of symmetry. One of the phosphorus atoms is close to the anellated benzene moiety of the indenyl ligand, while the other one is further away, on the less congested side of the compound. ^1H NMR spectroscopic data (Table 7) and ^{13}C NMR spectroscopic data (see Experimental Section) are in agreement with the given formula (Table 11). By an extensive series of NMR experiments, it was proved (see below) that the signal at $\delta = 30.4$ can be assigned to the phosphorus nucleus which lies below the anellated benzene ring.

With **4b** as the ligand constituent of **16b**, two diastereomeric forms of **16b** could be expected: one with the anellated ring on the side of the PPh_2 group and a second with the PEt_2 group and the anellated ring close to each other. From the ^{31}P NMR spectroscopic data of **16b**, it appeared that only one of these isomers was formed (Table 7). In order to find out which of the two possible isomers was formed,

since it was not possible to grow single crystals of **16**, the structures of **16a** and **16b** were elucidated by NMR experiments.

NMR Analysis

Compound **16a** shows a well-resolved ^1H NMR spectrum (Figure 4 and Table 7). Filtering this spectrum by means of long-range phosphorus coupling led to the lower traces shown in Figure 4. The signals of the methylene protons, as well as the signals of the aromatic protons are clearly differentiated by these traces. $^2J_{\text{HP}}$ coupling leads to prominent signals for the methylene groups which are directly bonded to the phosphorus nuclei. The protons of the methylene groups are diastereotopic owing to the lack of symmetry of the compound as a whole. This diastereotopicity is apparent from the characteristic doublet of doublets for each of the protons of the methylene groups linked to the phosphorus atom. The signals labelled $\text{H}^{1\text{a}}/\text{H}^{1\text{b}}$

H^{1B} (Figure 4 and Figure 6) are therefore assigned to the methylene group at P^1 , the ones labelled H^{2A}/H^{2B} (Figure 4 and Figure 6) originate from the methylene group at P^2 . The remaining signals H^{3A}/H^{3B} (Figure 4 and Figure 6) must therefore be due to the CH_2Cp group. The $CH_2O-SiMe_3$ group (Figure 4 and Figure 6) gives rise to signals at $\delta = 3.85$ and 0.36 .

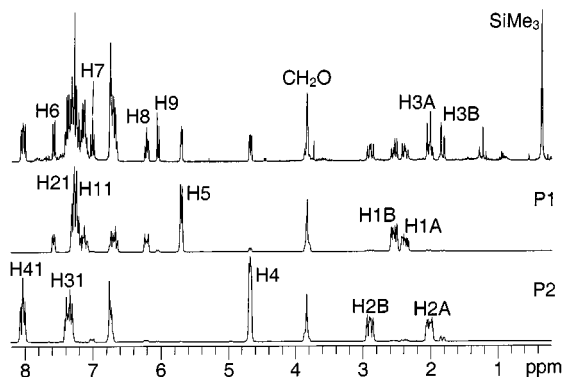


Figure 4. 1H NMR spectrum (top) and cross-sections of the $\{^1H, ^{31}P\}$ -HMBC spectrum of **16a**; centre trace: filtering by long-range coupling to P^1 ; bottom trace: filtering by long-range coupling to P^2

The parts of the spectrum assigned to the protons of the Cp moiety are less conclusive: There are different pathways along which ^{31}P coupling to these protons may occur, while for the methylene protons $^2J_{HP}$ coupling is the dominant pathway. It is interesting to note that one of the Cp protons (H^5 ; Figure 4 and Figure 6) correlates strongly with P^1 , while the other shows a strong correlation with P^2 (H^4 ; Figure 4 and Figure 6).

The aromatic protons are as well differentiated by their different correlations with P^1 and P^2 (Figure 4 and Figure 6). Unambiguous assignment was not possible from this experiment alone and the assignment given in Figure 4 was based on additional experimental grounds. A plausible argument for assigning the signal H^{41} (Figure 4 and Figure 6) comes from comparison with the NMR spectroscopic behaviour of other tripod metal compounds:^[15,18] In the aryl region of the 1H NMR spectra of such compounds, the signals with the greatest downfield shift have always been found to be due to the *ortho*-protons of phosphorus-bonded phenyl rings, wherever assignment was possible. The well-separated signal observed for H^{41} in the aromatic region (Figure 4 and Figure 6) together with its downfield shift allowed for its assignment to an *ortho*-proton of a phenyl

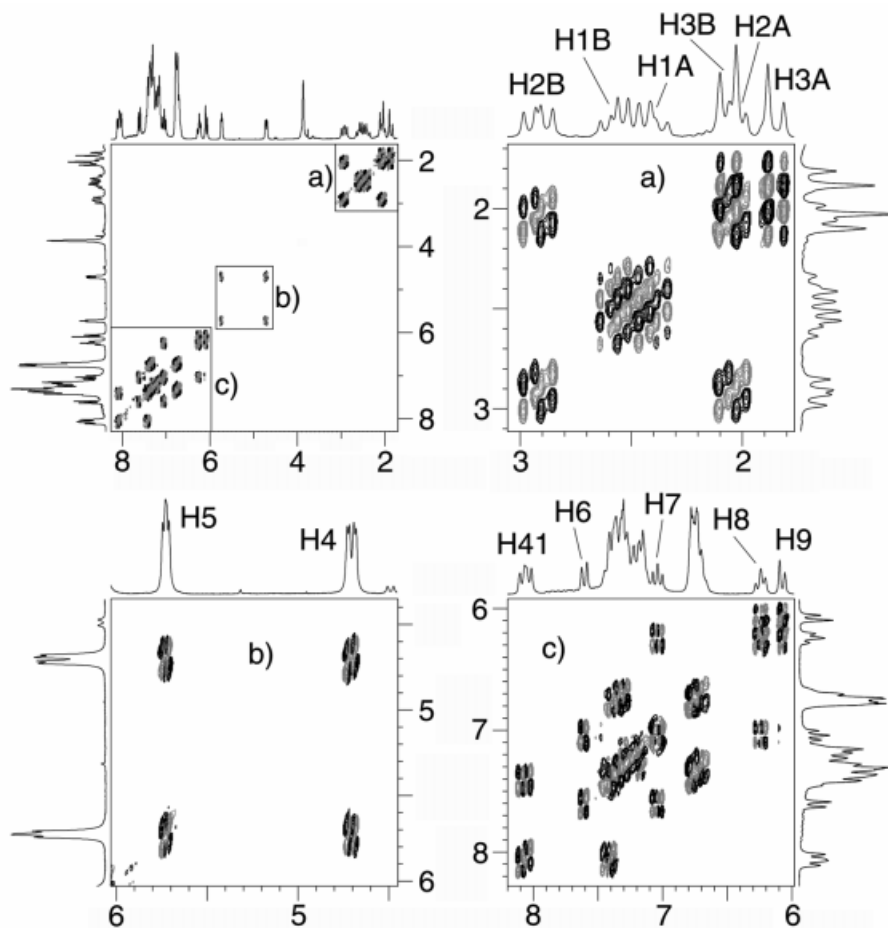


Figure 5. DQF-COSY spectrum of **16a**; the individual regions labelled a, b, and c in the complete spectrum (top left) are shown in magnified form under these labels

ring bonded to P². ³¹P-decoupling reduced the doublet of doublet structure of this signal (Figure 4) to a well-resolved doublet, as expected.

The assignment of the individual signals in the methylene region was confirmed by COSY experiments. These experiments revealed the individual methylene groups by their ²J_{HH} coupling (Figure 5a).

COSY data were important for the unambiguous assignment of resonances to the indenyl part of the molecule. While the Cp part of the indenyl ligand was clearly appar-

ent even from 1D NMR experiments (Figure 4, see above), the signals of the protons H⁶–H⁹ (Figure 4, Figure 5 and Figure 6) in the anellated benzene ring of the indenyl fragment, while apparent as individual patterns, could not be assigned with respect to their mutual sequence. The COSY spectrum shown in Figure 5 (5c) enabled the sorting of the signals into a sequence of mutually neighbouring protons. The only ambiguity remaining was the question as to which of the protons, H⁶ or H⁹, was at the back or the front of the molecule (Figure 6). This ambiguity was resolved by NOE

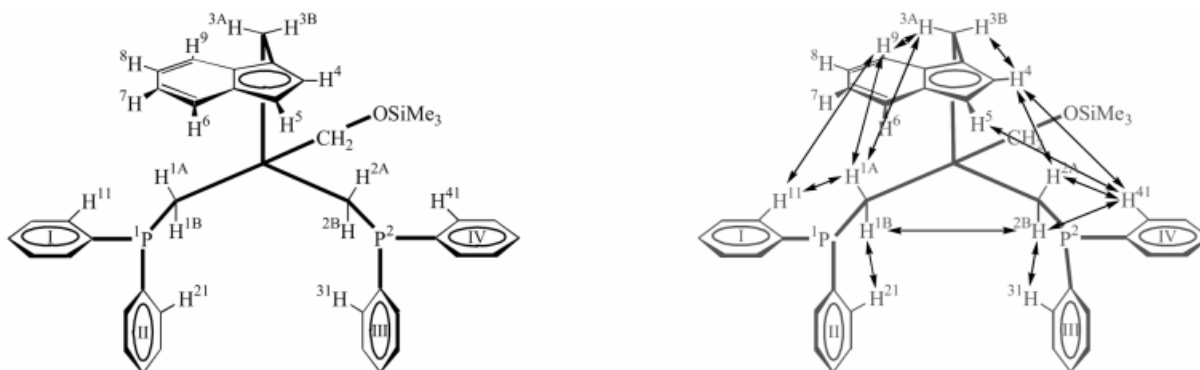


Figure 6. Numbering scheme used in the NMR analysis of **16a**; the right hand side shows the conformationally relevant and experimentally accessible NOE contacts as double-headed arrows

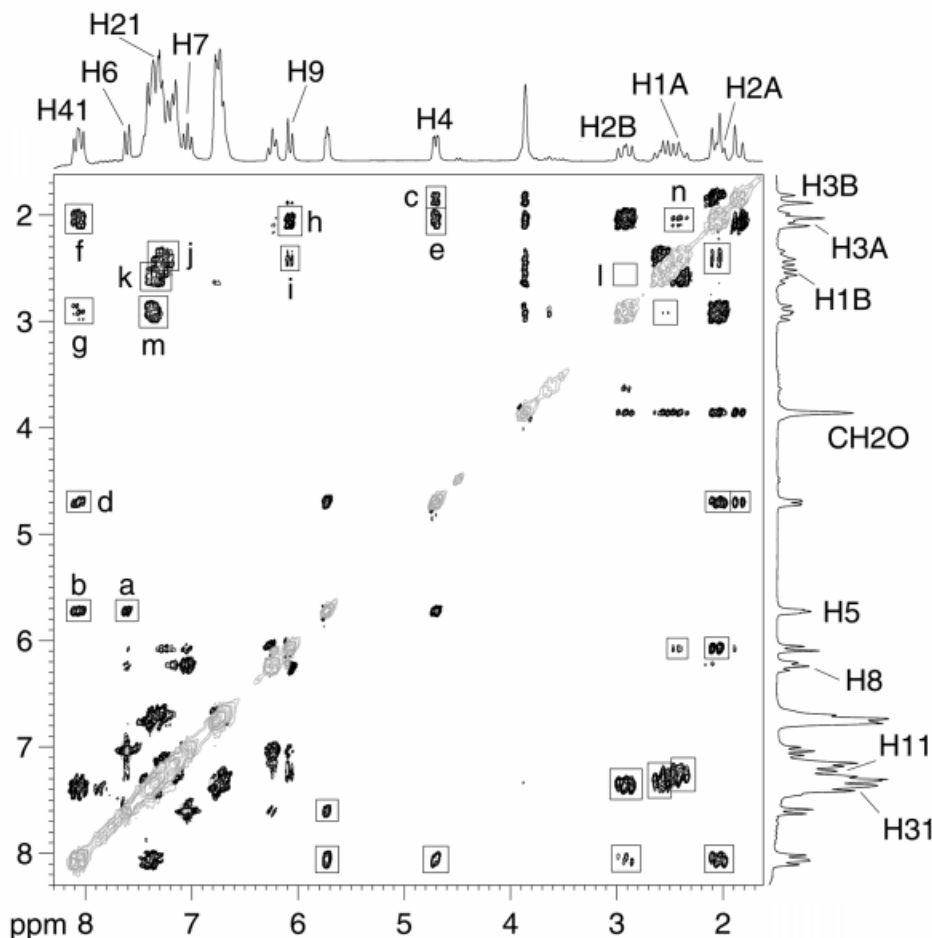


Figure 7. NOESY spectrum of **16a**; the labels designating individual conformationally relevant cross-peaks are used as an abbreviated reference in the text; the origin of the cross-peaks follows from the labelling of the spectral traces

experiments (Figure 7),^[19] which finally allowed for the unambiguous assignment of all the conformationally relevant protons labelled in Figure 6. The ambiguity about the position of the protons H⁶/H⁹ was resolved by the observation of a strong cross-peak (Figure 7; labelled a) between one of the protons of the Cp part of the ligand (H⁵) and one of the protons of the anellated benzene moiety (H⁶). The position of both protons (referring to Figure 6) is clear from this observation.

H⁵ shows a correlation with H⁴¹ (Figure 7; b) while H⁴ shows correlations with H^{3b}, H⁴¹ and H^{2A} (Figure 7; c, d, e). H^{2A} itself correlates with H⁴¹ (Figure 7; f) and H⁴¹ shows a cross-peak with H^{2B} (Figure 7; g), which also correlates with H³¹ (Figure 7; m). These correlations built up a framework which unambiguously differentiated between the two sides of the compound and showed that the phosphorus atom labelled P² was at the side of the molecule opposite to that containing the anellated benzene ring (Figure 6).

The mutual orientation of the constituents at the other side of the molecule may be inferred from cross-peaks between H⁹ and the methylene protons H^{3A} and H^{1A} (Figure 7; h, i). H^{1A} correlates with H¹¹ and with H^{3A} (Figure 7; j, n). The second proton of this methylene group H^{1B}, shows a cross-peak with H²¹ as well as with H^{2b} (Figure 7; k, l). Some additional correlations involving *meta*-protons are also observed (Table 8). A scaffolding was thus apparent from the NOE experiments which qualitatively completely defined the conformation of **16a** (Figure 6, right-hand side).

A quantitative insight into the conformational manifold adopted by **16a** in solution was provided by a molecular modelling approach. To this end, a model representation was constructed. The basic geometry may be taken from the experimental structures of similar compounds such as H₃CC(CH₂-η¹-PPh₂)₂(CH₂-η⁵-Cp)RuCl^[15] with the anellated benzene moiety and the TMS group being added by modelling procedures.^[20] The model thus generated was locally optimised with respect to energy as a template for any further calculations. Alternatively, the model may be constructed without explicit reference to similar molecules by using the parameters of the modelling package (Discover 3.0, ESFF force field) alone. Both these approaches led to basically the same conformations of the model template.

As was also observed in the structures of Cp derivatives H₃CC(CH₂-η¹-PPh₂)₂(CH₂-η⁵-Cp)RuCl, the chelate cage itself is chiral.^[15] The torsion angles Ru–P–CH₂–C_{*ipso*} never conform to a mirror symmetric arrangement, even in the case of Cp derivatives.^[2,3,6,15] With the indenyl ligand of **16a**, additional side differentiation was imposed on the molecules such that conformational diastereomers may exist. To cope with this problem, starting from the model compound, a second model was constructed leaving everything unchanged besides the orientation of the indenyl group which was rotated around its C–CH₂ axis by 180°. These two diastereomeric model templates, together with the quantitative information of the inter-proton distances were used for distance-geometry (DG) calculations.^[21] From these procedures, a set of conformations resulted,

Table 8. NOE contacts in **16a**

No. ^[a]	16a		<i>d</i> _{NOE} [pm]	<i>d</i> _{calcd.} [pm]	σ ² [pm ²]
1	H1A	H1B	251	177	5476
2	H2A	H2B	206	176	900
3	H3A	H3B	218	176	1764
4	H4	H5	253	265	144
5	H5	H6	278	295	289
6	H6	H7	230	242	144
7	H7	H8	234	256	484
8	H8	H9	245	240	25
9	H41	H42	201	247	2116
10	CH ₂ OSi	H1A	289	245	1936
11	CH ₂ OSi	H1B	300	308	64
12	CH ₂ OSi	H2B	302	291	121
13	CH ₂ OSi	H3A	270	246	576
14	CH ₂ OSi	H3B	281	239	1764
15	H1A	H3A	304	254	2500
16	H1A	H11	226	209	289
17	H1A	H9	318	319	1
18	H1B	H2B	361	274	7517
19	H1B	H21	229	232	9
20	H2A	H4	260	268	64
21	H2A	H41	247	247	0
22	H2B	H41	305	265	1600
23	H2B	H31	226	213	169
24	H3A	H9	256	245	121
25	H3B	H4	290	278	144
26	H4	H41	280	296	256
27	H4	H42	370	437	4489
28	H5	H41	259	245	196
29	H8	H12	289	363	5476
30	H9	H11	298	318	400
Contacts No.		1–9	1–30	10–30	15–30
RMS [pm]		35	36	36	38

^[a] Atom labels refer to Figure 6 throughout. H42 (No. 27) and H12 (No. 29) designate protons in the *meta* position of the aryl rings IV and I, respectively. Contacts No. 1–9 refer to distances which are fixed by the covalent framework. In the final calculations, contacts No. 2 and 4 were used as reference distances to transform the NOE volume integrals into distances. Contacts No. 10–14 designate distances which are not fixed by the covalent framework but refer to CH₂ protons of the CH₂OSi fragment which are diastereotopically not differentiated in the spectra. The “dummy atom” approach was used to incorporate these contacts in the calculations.^[29] Contacts No. 15–30 are also not fixed by the covalent framework and build up a tight scaffolding to which the conformation has to adopt. The *ortho* and *meta* protons of the aryl groups show no diastereotopic differentiation in the spectra. For the purpose of distance-geometry calculations, each pair of these protons was replaced by a dummy atom.^[29] For the purpose of energy minimisation and rms calculation, the protons were assigned individually with respect to whichever one gave the shorter distance. The rms values given refer to inter-proton distances exclusively. The set of contacts to which they refer is indicated by the appropriate range in terms of their numeric labels. Since contacts No. 1–9 refer to distances which are fixed by covalent bonding, the respective rms value presents an expected value for the overall accuracy. The rms values referring to all contacts (No. 1–30) or only to conformationally relevant subsets (No. 10–30, No. 15–30) are well within the expected range.

which were in agreement with the restraints imposed by the distances pertaining to the model and by the inter-proton distances from the NOE data.

Figure 8 shows the results obtained for **16a**. The ten conformations (grey) with the lowest distance violations (with the best overall agreement) are shown. While it is clear from the NMR observations that the phenyl groups are free to

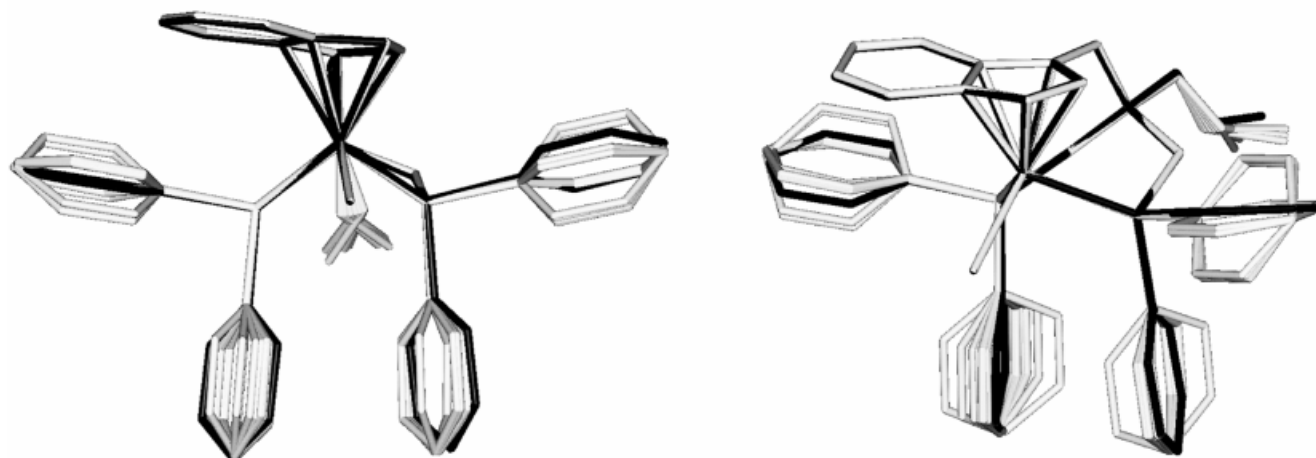


Figure 8. NMR-derived conformations characterising **16a** in solution; the conformation shown in black represents the optimal single conformation

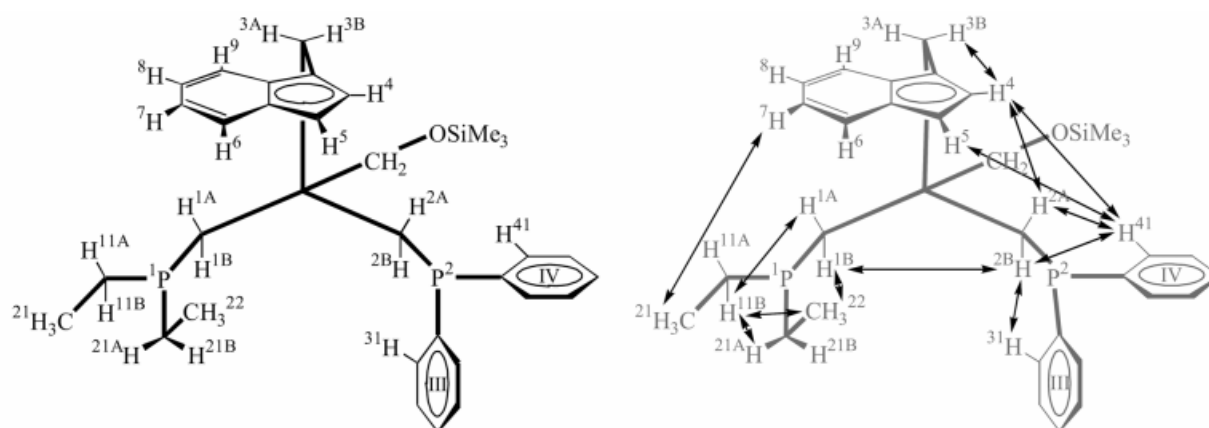


Figure 9. Numbering scheme used in the NMR analysis of **16b**; the right-hand side shows the conformationally relevant and experimentally accessible NOE contacts as double-headed arrows

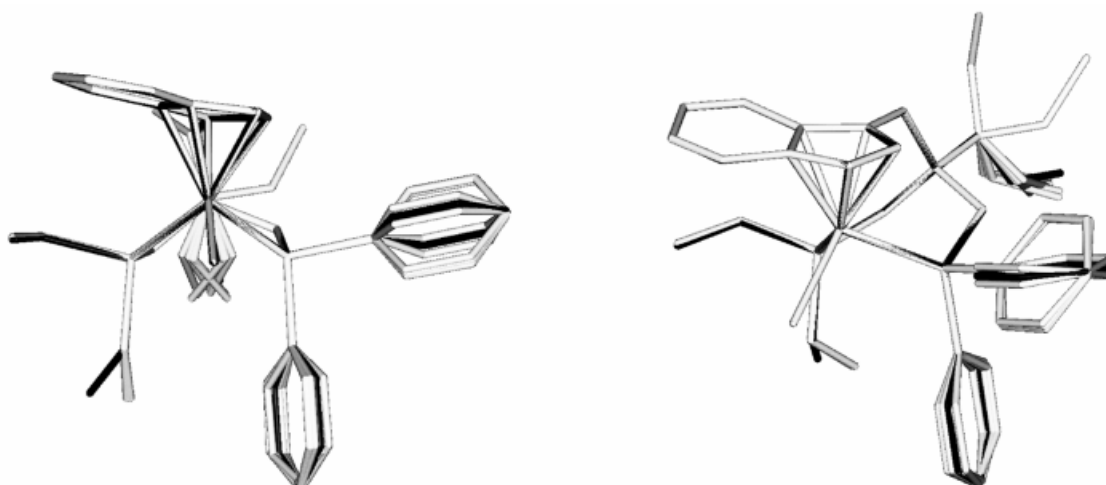


Figure 10. NMR-derived conformations characterising **16b** in solution; the conformation shown in black represents the optimal single conformation

rotate (only one H_{ortho} signal for each of the four phenyl groups was observed) a rotational preference is apparent from the distance-geometry results (Figure 8). From this set

of conformations, obtained by distance-geometry calculations, the one with the best agreement was used to define the starting structure for geometry optimisation on the ba-

Table 9. NOE contacts in **16b**

No. ^[a]	16b		d_{NOE} [pm]	$d_{\text{calcd.}}$ [pm]	σ^2 [pm ²]
1	H1A	H1B	185	177	64
2	H2A	H2B	195	176	350
3	H3A	H3B	272	176	9293
4	H4	H5	250	265	237
5	H5	H6	277	295	310
6	H6	H7	233	242	74
7	H11A	H11B	197	176	458
8	H11B	H12	271	248	520
9	H21A	H21B	183	175	66
10	H21A	H22	265	248	292
11	H41	H42	210	246	1332
12	CH ₂ OSi	H1A	270	243	708
13	CH ₂ OSi	H1B	296	315	372
14	CH ₂ OSi	H2A	272	257	210
15	CH ₂ OSi	H2B	274	289	219
16	CH ₂ OSi	H3B	237	236	1
17	H1A	H11B	242	267	650
18	H1B	H2B	295	272	506
19	H1B	H22	282	223	3505
20	H2A	H4	230	246	262
21	H2A	H41	247	249	5
22	H2B	H41	269	258	130
23	H2B	H31	220	209	121
24	H3B	H4	299	285	196
25	H4	H41	280	314	1156
26	H5	H41	251	242	79
27	H7	H12	296	337	1706
28	H11B	H21A	239	310	5055
29	H11B	H22	263	224	1552
Contacts No.	1–11	1–29	12–29	17–29	
RMS [pm]	34	32	30	34	

^[a] Atom labels refer to Figure 9 throughout. The meaning of columns and designations is analogous to the one explicitly described for **16a** in Table 8. Contacts No. 1, 2, 4, and 7 were used as the distance reference.

sis of energy minimisation. The resulting minimised conformation is shown in black in Figure 8.

With the best model from distance-geometry alone, the rms deviation between the observed and calculated distances is only approximately 3 pm. This traditional measure of quality of agreement between calculated conformations and NOE distances is quite biased, since the distances determined by the covalent framework and the distances referring to NOE contacts are measured by the same ruler. It appears more appropriate to consider the difference between NOE-derived distances and their computationally generated counterparts alone to derive a measure of quality. For the model generated by distance-geometry, this measure results in an rms of 48 pm. With the optimal conformation obtained after energy minimisation, this rms deviation is approximately 36 pm and thus corresponds to the error estimated for the accuracy of the NOE distances (Table 8).

The procedure as described for the NMR analysis of **16a** was also applied to **16b**. ¹H-, ³¹P-HMBC^[22] and ¹H-, ¹H-COSY experiments together with other 2D NMR spectroscopic data did allow for the complete assignment of an extensive subset of signals (Table 7, Figure 9 and Experimental Section).

The measured NOE contacts built up a tight scaffolding which the conformation of **16b** had to adopt (Figure 9, right-hand side). The NMR spectroscopic data also clearly showed that **16b** was diastereomerically pure. If there were another diastereomer present, its concentration must be below the NMR detectable limit (< 1%). It is clear from these experiments that the phosphorus nucleus of the PET₂ group resonates upfield (P¹, δ = 33.8, Table 7) from that of the PPh₂ group (P², δ = 56.3, Table 7). It is also clear that the PET₂ group is located on the same side as the anellated benzene ring. Refinement of the structure by the same procedures applied to **16a** led to the set of conformations shown in Figure 10.

The optimal single conformation is shown in black in Figure 10. The rms deviation between the calculated and experimental values of 18 conformationally relevant interproton distances (Figure 9) is only 30 pm (Table 9). This single conformation is therefore in optimal agreement with the NOE data. The most important result of this NMR analysis is that it proves that chiral indenyl-containing *tripod* ligands form their *tripod* metal derivatives under complete diastereoselective control.

Conclusion

Functionalised tripod ligands of the type ROCH₂C(CH₂PPh₂)(CH₂PR'₂)(CH₂Cp[#]) (Cp[#] = indenyl, fluorenyl) are accessible from the oxetane precursor O(CH₂)₂C(CH₂Br)(CH₂OMs) in a few steps. These tripod ligands form ruthenium complexes of the CpRuL₂Cl type with the Cp[#] group and the phosphorus donor groups linked by a *neo*-pentane scaffolding.

Epichlorohydrin is a suitable starting material to prepare chelate ligands (Cp[#]CH₂)CHOH(CH₂PPh₂) in fully diastereoselective one-pot syntheses. These chelate ligands coordinate highly diastereoselectively to Ru(PPh₃)(Cl).

The formation of the complex Me₃SiOCH₂C(CH₂- η^1 -PPh₂)(CH₂- η^1 -PET₂)(CH₂- η^5 -Indenyl)RuCl is completely diastereoselective, with the six-membered cycle of the indenyl constituent lying on the same side to which the PET₂ group is coordinated.

A complete and unambiguous structure analysis of the *tripod* compounds Me₃SiOCH₂C(CH₂- η^1 -PPh₂)(CH₂- η^1 -PR₂)(CH₂- η^5 -Indenyl)RuCl (R = Ph, Et) by a combination of NMR spectroscopy methods as well as distance-geometry modelling is reported, which documents the power of NMR methods for the quantitative analysis of structures of coordination compounds.

Experimental Section

General Remarks: All manipulations involving phosphanes were carried out under argon by means of standard Schlenk techniques and were monitored by TLC (Macherey–Nagel Co., Polygram SIL G/UV₂₅₄). All solvents were dried by standard methods^[23] and distilled under argon. The solvents CDCl₃ and CD₂Cl₂ used for NMR spectroscopic measurements were degassed by three successive

“freeze-pump-thaw” cycles and dried over 4-Å molecular sieves. – MS: Finnigan MAT 8320; EI (70 eV); FAB (Xenon; matrix: 4-nitrobenzyl alcohol). – HR-MS(EI): Jeol JMS-700. – HR-MS(FAB): VG ZAB 2F – Melting points: Gallenkamp MFB-595 010; uncorrected values. – Optical rotations: Jasco DIP310, 10-cm cell, Na-D line ($\lambda = 589$ nm) – Cyclovoltammetry: EG&G Princeton Applied Research model 273; potentials in mV versus SCE at a glassy carbon electrode at 25 °C; solutions of compounds: 10^{-3} M in 0.1 M Bu_4NPF_6 in CH_2Cl_2 . – Elemental analyses: Microanalytical Laboratory of the Organisch-Chemisches Institut, Universität Heidelberg.

Materials: Silica gel (Kieselgel z. A. 0.06–0.2 mm, J. T. Baker Chemicals B. V.) used for chromatography was degassed at 1 mbar for 24 h and saturated with argon. A solution of $n\text{BuLi}$ in hexane (2.5 M) was used for deprotonations. *S*-(+)- and *R*-(-)-epichlorohydrin (**5**) (97% *ee*) were degassed and checked for optical purity by measurement of their specific rotations ($[\alpha]_D^{20} = 34.3^{[24]}$). HPeEt_2 ,^[25] HPPPh_2 ,^[26] 3-(bromomethyl)-3-(methanesulfonoxymethyl)oxetane (**1**),^[5] 1,1-bis(diphenylphosphanylmethyl)-1-(cyclopentadienylmethyl)ethane,^[2b] $(\text{PPh}_3)_2\text{FeCl}_2$ ^[10] and $(\text{PPh}_3)_3\text{RuCl}_2$ ^[27] were prepared according to or by adaptation of literature procedures. All other chemicals were obtained from commercial suppliers and used without further purification.

NMR: Spectra were recorded at 298 K with a Bruker Avance DPX200 spectrometer at 200.13 MHz (^1H), 50.323 MHz (^{13}C), 81.014 MHz (^{31}P) and with a Bruker Avance DRX300 spectrometer at 300.13 MHz (^1H), 121.495 MHz (^{31}P); chemical shifts (δ) are reported in ppm with CHCl_3 (^1H : $\delta = 5.32$; ^{13}C : $\delta = 53.5$) as internal standard; ^{31}P chemical shifts (δ) are reported in ppm with 85% H_3PO_4 (^{31}P : $\delta = 0$) as external standard. Acronyms of pulse programmes refer to pulse sequences supplied under these names for the BRUKER series of instruments; relaxation delays for 2D NMR experiments were set at around 1.5 s if not stated otherwise. ^1H - ^{31}P -HMBC: pulse sequence inv4gslnrd; instruments DRX300 (**16a**), DPX200 (**16b**); spectral width $F_2 = 2588$ Hz, $F_1 = 3888$ Hz (**16a**), $F_2 = 1717$ Hz, $F_1 = 2755$ Hz (**16b**), mixing time 70 ms. ^1H , ^{13}C -HMBC: pulse sequence inv4gslnrd; instrument DPX200; spectral width $F_2 = 1380$ Hz, $F_1 = 6542$ Hz (**16a**), $F_2 = 1717$ Hz, $F_1 = 7348$ Hz (**16b**), mixing time 70 ms. ^1H , ^{13}C -HSQC: pulse sequence invieagssi; instrument DPX200; spectral width $F_2 = 1380$ Hz, $F_1 = 6542$ Hz (**16a**), $F_2 = 1717$ Hz, $F_1 = 7046$ Hz (**16b**). ^1H , ^1H -DQFCOSY: pulse sequence cosygsmft; instrument DPX200; spectral width 1380 Hz (**16a**), 1717 Hz (**16b**) in both dimensions. ^1H , ^1H -NOESY: pulse sequence noesypt; instrument DPX200; spectral width 1380 Hz (**16a**), 1717 Hz (**16b**) in both dimensions; relaxation delay 2.0 s; mixing time 500 ms.

NOE Analysis: The NOE peaks were integrated by standard methods (volume integration, Felix software package from MSI).^[20,28] The peak volumes were transformed to distances by assuming the initial rate approximation to be valid. For bringing the distances to an absolute scale, the known inter-proton distances of H^4/H^5 (265 pm) and $\text{H}^{2A}/\text{H}^{2B}$ (178 pm) (**16a**) and $\text{H}^{1A}/\text{H}^{1B}$, $\text{H}^{2A}/\text{H}^{2B}$, $\text{H}^{11A}/\text{H}^{11B}$ (178 pm) and H^4/H^5 (265 pm) (**16b**) were used. Other combinations of reference distances were also tested; different sets of references did not cause changes greater than 10%. Owing to the fact that only one mixing time was used, the overall accuracy of the NOE-derived distances will not be much better than 30 pm.

Distance-Geometry Calculations: The NOE-derived distances were used to build the distance matrix, together with the distance limits derived from covalent bonding. Upper and lower boundaries for

NOE distances were set at 10%. The distance restraints derived from covalent bonding were defined by the DGII programme package (DGII package of NMR Refine module, InsightII, 98.0).^[20b] Some of the protons, the *ortho*- and *meta*-protons of the phenyl groups and the protons of the $\text{CH}_2\text{OSiMe}_3$ group had to be replaced by dummy atoms since no diastereotopic differentiation was apparent for these protons. The upper boundary of the distance interval referring to these dummy protons was appropriately increased by 100 pm.^[29] Distance-geometry calculations were used to produce a total of 200 conformations for each of the compounds **16a** and **16b**. The starting models were based on the structures obtained in each case by energy minimisation. In order to efficiently cope with the problem caused by the conformational chirality of the cage, the mirror image of this model with respect to the torsions within this cage was also incorporated as a starting point. Each of these two starting structures for each of the compounds **16a** and **16b** was allowed to adapt to the NOE restraints (DGII package of NMR Refine module, Insight98.0).^[20b] The number of different conformations resulting from this procedure was limited to 100 for each starting geometry. It was observed that the minimisation procedure was able to converge from one sense of skew of the scaffolding to its opposite. Repetitive runs, however, showed that the degree of skewness of the chelate cage of the resulting structures was highly biased by the degree of skewness of the starting structure. This problem was overcome by the technique described above. With respect to the torsion angles $\text{Ru}-\text{P}-\text{CH}_2-\text{C}_{\text{ipso}}$, the DGII runs produce solutions which are close to being either symmetric with respect to the idealised mirror plane (bisecting the $\text{P}-\text{Ru}-\text{P}$ angle and vertical to the $\text{P}-\text{Ru}-\text{P}$ plane) or are antisymmetric with respect to this plane. With respect to energy minimisation calculations (see below) the best solutions for these torsional arrangements were used as a starting point. From the 200 conformations generated for both **16a** and **16b**, the 10 with the best overall agreement were selected to produce the superposition graphs shown in Figure 8 and Figure 10. In order to construct a model which best approximates the NOE distances and at the same time corresponds to a local minimum of the force field generated molecular hypersurface, the following procedure was adopted. Energy minimisation of the best structures generated by distance-geometry was done with the distances determined by NOE measurements constrained by corresponding high-force constants (harmonic potential force constants: $100 \text{ kcal}\cdot\text{mol}^{-1}\cdot\text{\AA}^{-2}$). After reaching convergence, the NOE-derived constraints were removed and the conformation was allowed to relax on the basis of the molecular force field alone. The rms deviation between the model with NOE restraints and the one without was found to be 37 pm (**16a**) and 26 pm (**16b**) (based on all atoms). The resulting conformations are shown in black in Figure 8 and Figure 10. Generating an optimal model by the alternative procedure of taking the best solutions from the DGII runs as the starting points for the force-field refinement (no additional NOE restraints) led to similar results. The optimal solution derived by constrained refinement was again found. The minima derived by both methods were the same for **16a** (rms = 1.6 pm, based on all atoms) and **16b** (rms = 1.7 pm, based on all atoms). As a measure of agreement between the models and the experimental values, the rms deviation between the distance estimates from the model and from the experiment was calculated. Different subsets of inter-proton distances were included in these calculations. As is seen in Table 8 and Table 9, the individual error estimates were very similar to each other, independent of which subset was chosen for their calculation.

Synthetic Procedures: The analytical data are collected in Table 10 and 11. NMR spectroscopic data, if not explicitly given in the experimental protocols are presented in Table 1–3, and Table 7.

Table 10. Analytical data of compounds 2–12

No.	Empirical formula (<i>M</i>)	Eluent ^[a] (<i>R_f</i>)	MS (EI) <i>m/z</i> (%) [Frag.]	C _{calcd.} , H _{calcd.} , P _{calcd.} C _{found} , H _{found} , P _{found}	M.p. ^[b] [°C]	HR-MS M _{calcd.} ⁺ /found	Yield (%)
2a	C ₂₆ H ₂₅ OP (384.46)	PE/Et ₂ O, 7:3 (0.33)	384 (100) [M ⁺]; 353 (52) [M ⁺ – CH ₂ O]; 199 (24) [M ⁺ – PPh ₂]	81.23, 6.55 80.64, 6.49	—	—	74
2b	C ₁₈ H ₂₅ OP (288.37)	PE/Et ₂ O, 7:3 (0.37)	288 (100) [M ⁺]; 259 (66) [M ⁺ – Et]; 258 (82) [M ⁺ – CH ₂ O]	74.97, 8.74 73.24, 8.53	—	—	10
2c	C ₃₀ H ₂₇ OP (434.52)	PE/Et ₂ O, 1:1 (0.47)	434 (89) [M ⁺]; 404 (2) [M ⁺ – CH ₂ O]; 269 (4) [M ⁺ – Fluorenyl]; 255 (3) [M ⁺ – CH ₂ Fluorenyl]	82.93, 6.26, 7.13 83.00, 6.58, 6.53	78	—	64
3a	C ₃₈ H ₃₆ OP ₂ (570.65)	PE/Et ₂ O, 3:2 (0.40)	571 (34) [M ⁺]; 494 (45) [M ⁺ – Ph]; 385 (100) [M ⁺ – PPh ₂]	79.98, 6.36, 10.86 79.18, 6.37, 10.84	80 (dec.)	—	73
3b	C ₃₀ H ₃₆ OP ₂ (474.56)	PE/Et ₂ O, 3:2 (0.48)	474 (12) [M ⁺]; 445 (100) [M ⁺ – Et]; 397 (7) [M ⁺ – Ph]; 385 (5) [M ⁺ – PEt ₂]; 289 (28) [M ⁺ – PPh ₂]	75.93, 7.65, 13.05 74.56, 7.50, 12.59	—	—	68
3c	C ₄₂ H ₃₈ OP ₂ (620.71)	PE/Et ₂ O, 6.5:3.5 (0.37)	620 (16) [M ⁺]; 544 (80) [M ⁺ – Ph]; 467 (30) [M ⁺ – 2Ph]; 435 (34) [M ⁺ – PPh ₂]	81.27, 6.17, 9.98 80.86, 6.40, 9.65	96	—	62
4a	C ₄₁ H ₄₄ OP ₂ Si (642.83)	PE/Et ₂ O, 9:1 (0.44)	642 (59) [M ⁺]; 566 (55) [M ⁺ – Ph]; 458 (100) [M ⁺ – PPh ₂]	76.60, 6.90, 9.65 75.75, 7.25, 9.76	—	—	86
4b	C ₃₃ H ₄₄ OP ₂ Si (546.74)	PE/Et ₂ O, 9:1 (0.41)	547 (6) [M ⁺]; 518 (100) [M ⁺ – Et]; 362 (15) [M ⁺ – PPh ₂]	72.49, 8.12, 11.34 72.38, 8.29, 11.26	—	—	84
4c	C ₄₅ H ₄₆ OP ₂ Si (692.89)	PE/Et ₂ O, 9:1 (0.49)	693 (31) [M ⁺]; 617 (85) [M ⁺ – Ph]; 405 (38) [M ⁺ – CH ₂ OTMS – PPh ₂]; 343 (19) [M ⁺ – PPh ₂ – Fluorenyl]; 329 (100) [M ⁺ – PPh ₂ – Fluorenyl – CH ₂]	78.01, 6.69, 8.94 78.02, 7.17, 8.77	—	—	38
6a	C ₂₀ H ₂₁ OP (308.36)	PE/Et ₂ O, 3:2 (0.37)	308 (63) [M ⁺]; 307 (24) [M ⁺ – H]	77.89, 6.87 74.02, 6.80	—	308.13300/ 308.13394	82
6b	C ₂₄ H ₂₃ OP (358.42)	PE/Et ₂ O, 1:1 (0.39)	358 (92) [M ⁺]	80.43, 6.47, 8.64 79.99, 6.50, 8.95	—	—	49
6c	C ₂₈ H ₂₅ OP (408.48)	PE/Et ₂ O, 3:2 (0.3)	408 (32) [M ⁺]	82.33, 6.17, 7.58 82.45, 6.13, 7.01	44	—	82
7	C ₂₁ H ₃₀ O (288.39)	PE/Et ₂ O, 1:1 (0.43)	288 (53) [M ⁺]; 270 (46) [M ⁺ – H ₂ O]; 159 (85) [M ⁺ – CH ₂ Indenyl]	87.46, 6.99 86.93, 7.00	61	—	4
8	C ₁₂ H ₁₂ O (172.22)	PE/Et ₂ O, 1:1 (0.22)	172 (22) [M ⁺]; 143 (13) [M ⁺ – COH]; 128 (100) [M ⁺ – CH ₂ CHOH]	83.69, 7.02 83.54, 7.13	—	—	30
9a	C ₂₃ H ₂₉ OPSi (380.54)	PE/Et ₂ O, 9:1 (0.72)	381 (62) [M ⁺]; 292 (13) [M ⁺ – OTMS]	72.59, 7.68, 8.14 71.01, 7.84, 8.16	—	380.1725/ 380.1729	96
9b	C ₂₇ H ₃₁ OPSi (430.60)	PE/Et ₂ O, 9:1 (0.56)	431 (66) [M ⁺]; 314 (100) [M ⁺ – Indenyl]	75.31, 7.26, 7.19 75.14, 7.41, 7.36	—	—	77
10	C ₂₀ H ₂₄ BOP (322.20)	PE/Et ₂ O, 3:2 (0.32)	321 (25) [M ⁺]; 308 (60) [M ⁺ – BH ₃]; 242 (10) [M ⁺ – CH ₂ Cp]; 108 (63) [M ⁺ – CH ₂ PPh ₂ BH ₃]	74.50, 7.51, 9.61 73.24, 7.54, 9.49	—	—	71
11	C ₂₁ H ₂₆ BO ₃ PS (400.29)	PE/Et ₂ O, 2:3 (0.37)	402 (5) [M ⁺]; 385 (4) [M ⁺ – BH ₃]; 370 (70) [M ⁺ – CH ₃ – BH ₃]; 305 (18) [M ⁺ – OSO ₂ CH ₃]; 291 (14) [M ⁺ – BH ₃ – OSO ₂ CH ₃]	62.98, 6.55, 7.74 60.63, 6.66	—	—	70
12a	C ₃₂ H ₃₀ OP ₂ (492.54)	PE/Et ₂ O, 9:1 (0.48)	492 (10) [M ⁺]; 307 (28) [M ⁺ – PPh ₂]; 291 (59) [M ⁺ – OPPh ₂]	78.03, 6.14, 12.58 75.92, 6.27	—	492.17719/ 492.18007	45
12b	C ₃₆ H ₃₂ OP ₂ (542.59)	PE/Et ₂ O, 4:1 (0.63)	542 (6) [M ⁺]; 357 (38) [M ⁺ – PPh ₂]; 341 (48) [M ⁺ – OPPh ₂]	79.69, 5.94, 11.42 79.49, 6.09, 11.36	—	—	51
12c	C ₄₀ H ₃₄ OP ₂ (592.65)	PE/Et ₂ O, 4:1 (0.59)	592 (12) [M ⁺]; 515 (20) [M ⁺ – Ph]; 427 (26) [M ⁺ – Fluorenyl]; 413 (94) [M ⁺ – CH ₂ Fluorenyl]; 391 (100) [M ⁺ – OPPh ₂]; 407 (29) [M ⁺ – PPh ₂]	81.07, 5.78, 10.45 81.07, 5.78, 9.90	97	—	61

^[a] PE = petroleum ether (boiling range 40–60 °C). – ^[b] dec. = decomposition.

Ligand Syntheses

General Procedure for the Synthesis of Compounds 2: The corresponding phosphane R_2PH (10 mmol) for the generation of the nucleophile **I** was dissolved in THF (50 mL) and deprotonated by the dropwise addition of $nBuLi$ (10 mmol) at 0 °C. This solution was stirred for 1 h at 25 °C. Meanwhile, nucleophile **II** (22 mmol, 2.2 equiv.) (indene or fluorene) was dissolved in THF (50 mL) and deprotonated in the same manner as nucleophile **I**. 3-(Bromomethyl)-3-(methanesulfonylmethyl)oxetane (**1**) (10 mmol) was dissolved in THF (50 mL) and cooled to –10 °C. At this temperature, the previously prepared phosphide (nucleophile **I**) solution was added dropwise over a period of 2 h. After the addition was completed, the mixture was allowed to warm to 25 °C and stirring was continued for another 30 min. Meanwhile the solution of nucleophile **II** was heated to 60 °C and the oxetane solution was added dropwise over a period of 1 h. The mixture was then heated at reflux for 2 h. After cooling to 25 °C, the mixture was hydrolysed by the addition of water (30 mL). The organic phase was separated, and the aqueous layer was extracted with diethyl ether (3×30 mL). The combined organic phases were washed with saturated NaCl solution until a neutral pH was achieved, and then dried with Na_2SO_4 . The solvent was evaporated in vacuo and the residue was purified by column chromatography (silica gel; eluent, R_f , yields, and analytical data as given in Table 10).

General Procedure for the Synthesis of Compounds 3: Phosphane R_2PH (6 mmol, 1.2 equiv.) for the generation of the nucleophile was dissolved in THF (40 mL) and deprotonated by the dropwise addition of $nBuLi$ (6 mmol) at 0 °C. This solution was stirred for 1 h at 25 °C. Meanwhile, oxetane **2** (5 mmol) was dissolved in THF (40 mL) and deprotonated in the same manner as the phosphane. The solution of the phosphide was added dropwise to the solution of the oxetane **2** over a period of 45 min at 25 °C. The resulting mixture was stirred for 3 h. The mixture was then heated at reflux for 2 h. After cooling to 25 °C the mixture was hydrolysed by the addition of water (30 mL). The organic phase was separated, and the aqueous layer was extracted with diethyl ether (3×30 mL). The combined organic phases were washed with saturated NaCl solution until a neutral pH was achieved, and then dried with Na_2SO_4 . The solvent was evaporated in vacuo and the residue was purified by column chromatography (silica gel; eluent, R_f , yields, and analytical data as given in Table 10).

General Procedure for the Synthesis of Compounds 4 and 9: The starting material (**3** or **6**) (4 mmol) was dissolved in CH_2Cl_2 (20 mL) and triethylamine (6 mmol, 1.5 equiv.) was added. The solution was cooled to 0 °C and trimethylsilyl chloride (5.2 mmol, 1.3 equiv.) was added dropwise. Stirring was continued for 1.5 h and then all volatiles were removed in vacuo. The remaining residue was further purified by column chromatography (silica gel; eluent, R_f , yields, and analytical data as given in Table 10).

General Procedure for the Synthesis of Compound 6a: Diphenylphosphane (10 mmol, 1 equiv.) was dissolved in THF (30 mL) and deprotonated by the dropwise addition of $nBuLi$ (10 mmol) at 0 °C. This solution was stirred for 1 h at 25 °C. Meanwhile, epichlorohydrin (10 mmol) was dissolved in THF (30 mL) and cooled to –70 °C. At this temperature, the phosphide solution was added dropwise over a period of 45 min. After warming to 25 °C, the solution was stirred for 30 min and added dropwise over a period of 20 min to a solution of $CpMgCl \cdot 2THF$ (23 mmol, 2.3 equiv.) in THF (40 mL). The resulting mixture was stirred for 15 h at 25 °C. The mixture was hydrolysed by the addition of an NH_4Cl solution (10%, 50 mL). The organic phase was separated, and the aqueous

layer was extracted with diethyl ether (3×30 mL). The combined organic phases were washed with a saturated NaCl solution until a neutral pH was achieved and then dried with Na_2SO_4 . The solvent was evaporated in vacuo and the residue was purified by column chromatography (silica gel; eluent, R_f , yields, and analytical data as given in Table 10).

General Procedure for the Synthesis of Compounds 6b/6c: Diphenylphosphane (10 mmol, 1 equiv.) for the generation of the nucleophile **I** was dissolved in THF (30 mL) and deprotonated by the dropwise addition of $nBuLi$ (10 mmol) at 0 °C. This solution was stirred for 1 h at 25 °C. Meanwhile, epichlorohydrin (10 mmol) was dissolved in THF (30 mL) and cooled to –70 °C. At this temperature, the solution of the phosphide was added dropwise over a period of 45 min. After warming to 25 °C, the solution was stirred for 30 min and added dropwise over a period of 20 min to a solution of nucleophile **II** (indenyllithium or fluorenyllithium, prepared in the same manner as nucleophile **I**) (23 mmol, 2.3 equiv.) in THF (40 mL). The resulting mixture was stirred for 15 h at 25 °C. The mixture was hydrolysed by the addition of water (30 mL). The organic phase was separated, and the aqueous layer was extracted with diethyl ether (3×30 mL). The combined organic phases were washed with a saturated NaCl solution until a neutral pH was achieved, and then dried with Na_2SO_4 . The solvent was evaporated in vacuo and the residue was purified by column chromatography (silica gel; eluent, R_f , yields, and analytical data as given in Table 10). The same procedure was used for the synthesis of $R(-)-$ **6b** from $S-(+)-$ **5** and $S-(+)-$ **6b** from $R(-)-$ **5**.

Procedure for the Synthesis of Compounds 7, 8: Indene (108 mmol) was dissolved in THF (40 mL). This solution was cooled to 0 °C and treated with $nBuLi$ (108 mmol). The solution was allowed to warm to 20 °C and stirred for 1.5 h. Meanwhile, epichlorohydrin (2.16 mmol) was dissolved in THF (20 mL) at –40 °C. The freshly prepared solution of $LiInd$ was added to this solution through a Teflon® capillary under a slight overpressure of Argon over 1 h. The resulting solution was stirred for 15 h at 20 °C. After hydrolysis with H_2O (30 mL), the organic phase was separated and the aqueous phase extracted with diethyl ether (3×30 mL). The combined organic phases were washed with a saturated NaCl solution until a neutral pH was achieved, and dried with $NaSO_4$. After evaporation of all volatiles in vacuo, the remaining material was dissolved in CH_2Cl_2 and separated by column chromatography (silica gel; eluent, R_f , yields, and analytical data as given in Table 10).

Procedure for the Synthesis of Compound 10: Compound **6a** (6.0 mmol) was dissolved in THF (40 mL). BH_3/THF (7.8 mL, 16.2 mmol) were added dropwise at 0 °C over 5 min. After stirring the solution for 1 h at 0 °C, the volatiles were removed in vacuo. The remaining colourless oil was dissolved in CH_2Cl_2 and purified by column chromatography (silica gel; eluent, R_f , yields, and analytical data as given in Table 10).

Procedure for the Synthesis of Compound 11: Compound **10** (6.0 mmol) was dissolved in CH_2Cl_2 (30 mL). After the addition of triethylamine (9 mmol), the solution was cooled to 0 °C. $MsCl$ (7.8 mmol) was added over 2 min and the solution was stirred for 6 h at 20 °C. After hydrolysis with H_2O (10 mL), the organic phase was separated. The aqueous phase was extracted with CH_2Cl_2 (3×20 mL). The combined organic phases were washed with a saturated NaCl solution until a neutral pH was achieved, and dried with $NaSO_4$. After evaporation of the solvent, the viscous oily residue was dissolved in CH_2Cl_2 and purified by column chromatography (silica gel; eluent, R_f , yields, and analytical data as given in Table 10).

General Procedure for the Synthesis of Compounds 12: Compound **6** (4 mmol) was dissolved in CH_2Cl_2 (20 mL) and triethylamine (5.6 mmol, 1.4 equiv.) was added. The solution was cooled to 0 °C and chlorodiphenylphosphane (4.8 mmol, 1.2 equiv.) was added dropwise. Stirring was continued for 2 h at 25 °C, and then all volatiles were removed in vacuo. The remaining residue was further purified by column chromatography (silica gel; eluent, R_f , yields, and analytical data as given in Table 10).

Syntheses of Coordination Compounds

General Procedure for the Synthesis of Compounds 13: Compound **9** (1 mmol) was dissolved in THF (20 mL) and deprotonated by the dropwise addition of $n\text{BuLi}$ (1 mmol) at 0 °C. The solution was stirred for 1.5 h at 25 °C. Meanwhile, FeCl_2 (0.6 mmol) was suspended in THF (15 mL) and stirred for 30 min. This solution was added dropwise to the solution of the deprotonated ligand over a period of 10 min. The mixture was stirred for 1 h. After this time, the mixture was heated, in the case of **13a**, for 4 h at reflux, and in the case of **13b**, for 2 h at 50 °C. All volatiles were removed in vacuo and the remaining residue was further purified by column chromatography. In the case of **13a**, the remaining residue was taken up in diethyl ether and purified by chromatography on neutral Al_2O_3 (Brockmann activity grade III). On evaporation of the solvent from the eluate, the purified compound **13a** was obtained in oily form. Further purification could be achieved by washing with petroleum ether (boiling range 40–60 °C) and resulted in a microcrystalline solid (Table 11). In the case of **13b**, the remaining

residue was purified by chromatography on neutral Al_2O_3 (Brockmann activity grade III). The contaminants were eluted with petroleum ether (boiling range 40–60 °C) and mixtures of petroleum ether/toluene. Subsequently, compound **13b** was eluted with toluene. On evaporation of the solvent from the eluate, the purified compound **13b** was obtained in microcrystalline form (Table 11).

^1H NMR: **13a** (CDCl_3): δ = –0.03 (s, 18 H, SiCH_3), 2.26 (m, 4 H, CH_2P), 2.58 (dd, 2 H, CH_{2a}Cp , $^2J_{\text{HH}}$ = 14.0 Hz, $^3J_{\text{HH}}$ = 6.0 Hz), 2.77 (dd, 2 H, CH_{2b}Cp , $^2J_{\text{HH}}$ = 14.0 Hz, $^3J_{\text{HH}}$ = 6.0 Hz), 3.72 (m, 2 H, CHOSi), 4.01 (br. s, 8 H, CpH), 7.30–7.50 (m, 20 H, aromatic CH). – **13b** (CDCl_3): δ = –0.25, –0.20 (2 s, 18 H, SiCH_3), 2.10–2.40 (m, 4 H, CH_2P), 2.55–3.40 (m, 4 H, $\text{CH}_2\text{Indenyl}$), 3.67 (m, 2 H, CHOSi), 3.80–4.10 (m, 2 H, Indenyl five-membered ring CH), 4.36 (m, 1 H, Indenyl five-membered ring CH), 4.48 (m, 1 H, Indenyl five-membered ring CH), 6.85–7.19 (m, 8 H, Indenyl six-membered ring CH), 7.19–7.55 (m, 20 H, aromatic H).

$^{13}\text{C}\{^1\text{H}\}$ NMR: **13a** (CDCl_3): δ = 0.6 (s, SiCH_3), 37.4 (d, CH_2P , $^1J_{\text{CP}}$ = 14.6 Hz), 39.6 (d, CH_2Cp , $^3J_{\text{CP}}$ = 8.5 Hz), 68.6, 68.7 (2 s, CpH (3, 4), 70.4, 71.0 [2 s, CpH (2, 5)], 72.3 (d, CHOSi , $^2J_{\text{CP}}$ = 17.6 Hz), 84.9 (s, *ipso*- C_q - Cp), 128.7–139.8 (aromatic C). – **13b** (CDCl_3): δ = 0.5 (s, SiCH_3), 36.0–38.1 (m, CH_2P and $\text{CH}_2\text{Indenyl}$), 60.7 (m, Indenyl five-membered ring CH), 61.5 (s, Indenyl five-membered ring CH), 71.7 (m, CHOSi), 73.4 (m, Indenyl five-membered ring CH), 75.8 (m, *ipso*- C_q -Indenyl five-membered ring), 87.1 (m, Indenyl five-membered ring C_q), 122.8–140.1 (aromatic and olefinic CH).

Table 11. Analytical data of compounds **13–16**

No.	Empirical formula (<i>M</i>)	MS <i>m/z</i> (%) [Frag.]	$\text{C}_{\text{calcd.}}$, $\text{H}_{\text{calcd.}}$, $\text{P}_{\text{calcd.}}$ C_{found} , H_{found} , P_{found}	$\text{M.p.}^{[a]}$ [°C]	HR-MS $\text{M}_{\text{calcd.}}^+/\text{found}$	Cyclovoltammetry Potential [mV] (SCE)	Yield (%)
13a	$\text{C}_{46}\text{H}_{56}\text{FeO}_2\text{P}_2\text{Si}_2$ (814.90)	<i>EI</i> 814 (18) [M^+]; 435 (100) [$\text{M}^+ - \text{C}_{23}\text{H}_{29}\text{OPSi}$]	67.80, 6.93, 7.60 68.00, 7.06, 7.84	–	–	$E_{1/2} = 325$; $\Delta E = 70$	86
13b	$\text{C}_{54}\text{H}_{60}\text{FeO}_2\text{P}_2\text{Si}_2$ (915.02)	<i>EI</i> 915 (8) [M^+]; 485 (100) [$\text{M}^+ - \text{C}_{27}\text{H}_{31}\text{OPSi}$]; 430 (54) [$\text{C}_{27}\text{H}_{31}\text{OPSi}$]	70.88, 6.61 69.70, 6.65	–	914.2956/ 914.2947	$E_{1/2} = 107$; $\Delta E = 283$	47
14	$\text{C}_{58}\text{H}_{53}\text{BClCoP}_2$ (917.20)	<i>FAB</i> 597 (100) [$\text{M}^+ - \text{BPh}_4$]; 562 (28) [$\text{M}^+ - \text{BPh}_4 - \text{Cl}$]; 503 (22) [$\text{M}^+ - \text{BPh}_4 - \text{Cl} - \text{Co}$]	75.95, 5.82, 6.75 73.31, 6.76, 6.14	–	–	–	38
15a	$\text{C}_{41}\text{H}_{43}\text{ClOP}_2\text{RuSi}$ (778.33)	<i>EI</i> 778 (4) [M^+]; 517 (18) [$\text{M}^+ - \text{PPh}_3$]; 481 (17) [$\text{M}^+ - \text{PPh}_3 - \text{Cl}$]	63.27, 5.57, 7.96 62.71, 5.90, 7.84	190 dec.	–	$E_{1/2} = 531$; $\Delta E = 160$	51
15b	$\text{C}_{45}\text{H}_{45}\text{ClOP}_2\text{RuSi}$ (828.39)	<i>FAB</i> 828 (80) [M^+]; 793 (100) [$\text{M}^+ - \text{Cl}$]	65.21, 5.48 64.60, 5.93	176 dec.	828.1447/ 793.1758, 828.1443/ 793.1777	$E_{1/2} = 429$; $\Delta E = 92$	36
16a	$\text{C}_{41}\text{H}_{43}\text{ClOP}_2\text{SiRu}$ (778.32)	<i>FAB</i> 778 (70) [M^+]; 743 (100) [$\text{M}^+ - \text{Cl}$]	63.22, 5.57 61.61, 5.67	160 dec.	778.1290/ 743.1602, 778.1306/ 743.1642	$E_{1/2} = 276$; $\Delta E = 73$	42
16b	$\text{C}_{33}\text{H}_{43}\text{ClOP}_2\text{RuSi}$ (682.25)	<i>FAB</i> 682 (100) [M^+]	–	154 dec.	682.1290/ 647.1602, 682.1266/ 647.1589	$E_{1/2} = 231$; $\Delta E = 99$	16

^[a] dec. = decomposition.

$^{31}\text{P}\{^1\text{H}\}$ NMR: **13a** (CDCl_3): $\delta = -23.6$ (s). – **13b** (CDCl_3): $\delta = -23.5$ (s).

General Procedure for the Synthesis of Compound 14: 1,1-Bis-(diphenylphosphanylmethyl)-1-(cyclopentadienylmethyl)ethane (1 mmol) was dissolved in THF (20 mL) and deprotonated by the dropwise addition of *n*BuLi (1 mmol) at 0 °C. The solution was stirred for 1.5 h at 25 °C. Meanwhile, CoCl_2 (1 mmol) was suspended in THF (20 mL) and cooled to -30 °C. The deprotonated ligand was added dropwise to this solution over a period of 5 min. After addition was completed, the mixture was allowed to warm to 20 °C and stirred for another 45 min. All volatiles were removed in vacuo. The remaining residue was dissolved in ethanol (20 mL) and NaBPh_4 (1 mmol) was added. After stirring for 2 h, all volatiles were removed in vacuo and the remaining residue was further purified by column chromatography. Compound **14** was eluted with THF/ CH_2Cl_2 mixtures. On evaporation of the solvent from the eluate, the purified compound **14** was obtained in microcrystalline form (Table 11).

^1H NMR: **14** (CD_2Cl_2): $\delta = 1.26$ (br. s, 2 H, CH_2Cp), 1.52 (br. s, 3 H, C_qCH_3), 2.29 (m, 2 H, CH_{2a}P , $^2J_{\text{HH}} = 15.7$ Hz), 2.59 (m, 2 H, CH_{2b}P , $^2J_{\text{HH}} = 15.7$ Hz), 4.68 (br. s, 2 H, Cp), 5.99 (br. s, 2 H, Cp), 6.75–7.95 (m, 60 H, aromatic CH).

$^{13}\text{C}\{^1\text{H}\}$ NMR: **14** (CD_2Cl_2): $\delta = 31.3$ (m, CH_2P), 33.3 (t, C_qCH_3 , $^3J_{\text{CP}} = 12.9$ Hz), 35.1 (s, CH_2Cp), 47.3 (s, C_q), 76.7, 97.9, 100.5 (3 s, Cp), 121.6–135.8 and 162.3–165.3 (m, aromatic CH).

$^{31}\text{P}\{^1\text{H}\}$ NMR: **14** (CD_2Cl_2): $\delta = 23.3$ (s).

General Procedure for the Synthesis of Compounds 15 and 16: The appropriate ligand (**4** or **9**) (1 mmol) was dissolved in THF (20 mL) and deprotonated by the dropwise addition of *n*BuLi (1 mmol) at 0 °C. This solution was stirred for 1.5 h at 25 °C. All volatiles were then removed in vacuo and the remaining residue was dissolved in 1,2-dichloroethane (1,2-DCE) (15 mL). This solution was added dropwise over a period of 10 min at 25 °C to a solution of $\text{RuCl}_2(\text{PPh}_3)_3$ (1 mmol) in 1,2-DCE (30 mL). The mixture was

stirred for 30 min. After this time, the mixture was heated for 2 h (**16**)/1.5 h (**15**) at 90 °C. All volatiles were removed in vacuo and the remaining residue was further purified by column chromatography. – **16** [solid phase neutral Al_2O_3 (Brockmann activity grade III)]: The excess triphenylphosphane and other contaminants were eluted with diethyl ether and the compounds **16** were subsequently eluted with $\text{Et}_2\text{O}/\text{CH}_2\text{Cl}_2$ mixtures. – **15** (solid phase silica gel): The excess triphenylphosphane and other contaminants were eluted with petroleum ether (boiling range 40–60 °C) (PE) and PE/ Et_2O mixtures. The compounds **15** were eluted with PE/ Et_2O 1:1. – On evaporation of the solvent from the eluate, the purified compounds **15** and **16** were obtained in microcrystalline form (Table 11).

^1H NMR: **15a** (CDCl_3): Major product: $\delta = -0.03$ (s, 9 H, SiCH_3), 1.73 (dd, 1 H, CH_{2a}Cp , $^2J_{\text{HH}} = 12.0$ Hz, $^3J_{\text{HH}} = 14.0$ Hz), 2.05 (dd, 1 H, CH_{2b}Cp , $^2J_{\text{HH}} = 12.0$ Hz, $^3J_{\text{HH}} = 12.0$ Hz), 2.55 (m, 2 H, CH_2P), 3.68 (m, 1 H, CHOSi), 3.73 (br. s, 1 H, Cp), 3.88 (br. s, 1 H, Cp), 4.52 (br. s, 1 H, Cp), 5.40 (br. s, 1 H, Cp), aromatic CH: 6.55–6.70 (m, 2 H), 6.86–6.94 (m, 2 H), 6.95–7.50 (m, 19 H), 8.05–8.20 (m, 2 H). – Minor product: $\delta = 4.97$ (s, 0.08 H, Cp), 5.18 (s, 0.08 H, Cp). – **15b** (CDCl_3): $\delta = 0.14$ (s, 9 H, SiCH_3), 2.78 (m, 2 H, CH_2P), 3.23 (m, 1 H, Indenyl five-membered ring CH, $^3J_{\text{HH}} = 2.2$ Hz), 3.28 (m, 1 H, $\text{CH}_{2a}\text{Indenyl}$), 3.70 (m, 1 H, $\text{CH}_{2b}\text{Indenyl}$, $J_{\text{HP}} = 7.6$ Hz), 4.08 (m, 1 H, CHOSi), 4.34 (m, 1 H, Indenyl five-membered ring CH, $^3J_{\text{HH}} = 2.2$ Hz), 6.80–7.70 (m, 29 H, aromatic and olefinic CH).

$^{13}\text{C}\{^1\text{H}\}$ NMR: **15a** (CDCl_3): Major product: $\delta = 0.5$ (s, SiCH_3), 33.2 (s, CH_2Cp), 37.0 (d, CH_2P , $^1J_{\text{CP}} = 28.1$ Hz), 68.6 (d, CHOSi , $^2J_{\text{CP}} = 12.5$ Hz), 74.4 (d, Cp, $J_{\text{CP}} = 10.0$ Hz), 76.6 (s, Cp), 78.2 (d, Cp, $J_{\text{CP}} = 11.0$ Hz), 84.7 (s, *ipso*- C_q -Cp), 99.8 (s, Cp), 127.6–135.9 (aromatic CH). **15b** (CDCl_3): $\delta = 0.6$ (s, SiCH_3), 32.5 (s, $\text{CH}_2\text{Indenyl}$), 39.2 (d, CH_2P , $^1J_{\text{CP}} = 29.7$ Hz), 65.0 (s, Indenyl five-membered ring CH), 69.1 (d, CHOSi , $^2J_{\text{CP}} = 9.5$ Hz), 73.6 (d, *ipso*- C_q -Indenyl five-membered ring, $J_{\text{CP}} = 13.6$ Hz), 83.9 (s, Indenyl five-membered ring CH), 104.7 (d, Indenyl five-membered ring C_q ,

Table 12. Crystal data for compounds **7**, **8**, and **15a**

Compound	7	<i>anti</i> - 8	15a ·2 CH_2Cl_2
Empirical formula	$\text{C}_{21}\text{H}_{20}\text{O}$	$\text{C}_{12}\text{H}_{12}\text{O}$	$\text{C}_{84}\text{H}_{90}\text{Cl}_6\text{O}_2\text{P}_4\text{Ru}_2\text{Si}_2$
Molecular mass	288.370	172.220	431.615
Crystal size [mm]	$0.05 \times 0.1 \times 0.2$	$0.07 \times 0.07 \times 0.2$	$0.15 \times 0.1 \times 0.03$
Crystal system	monoclinic	tetragonal	triclinic
Space group (No.) ^[31c]	$P2_1/n$ (14)	$P4_1$ (76)	$P\bar{1}$ (2)
Lattice constants:			
<i>a</i> [pm]	1645.0(3)	1260.6(2)	1001.3(2)
<i>b</i> [pm]	502.2(1)	1260.6(2)	1668.1(3)
<i>c</i> [pm]	1971.9(4)	604.4(1)	2473.6(5)
α [°]	90	90	100.69(3)
β [°]	109.63(3)	90	90.51(3)
γ [°]	90	90	101.10(3)
<i>V</i> [10 ⁶ pm ³]	1534	960.5	3980
<i>Z</i>	4	4	4
<i>d_x</i> [g cm ^{−3}]	1.248	1.191	1.441
<i>T</i> [K]	200	200	200
Scan range	$2.8^\circ \leq 2\theta \leq 52.1^\circ$	$3.2^\circ \leq 2\theta \leq 52.1^\circ$	$2.8^\circ \leq 2\theta \leq 52.0^\circ$
Method	ω scan, $\Delta\omega = 1.0^\circ$	ω scan, $\Delta\omega = 1.0^\circ$	ω scan, $\Delta\omega = 2.0^\circ$
Scan speed	40 s frame ^{−1}	30 s frame ^{−1}	25 s frame ^{−1}
No. of measured rflns.	11122	6580	57851
No. of unique rflns.	3003	1876	15570
No. of observed rflns.	2162	982	9344
Observation criterion	$I \geq 2\sigma$	$I \geq 2\sigma$	$I \geq 2\sigma$
No. of param. refined	259	154	911
Resid. el. density [10 ^{−6} e pm ^{−3}]	0.28	0.14	1.65
<i>R₁</i> / <i>R_w</i> [%] (refinement on <i>F</i> ²)	5.7/17.1	4.7/8.0	6.8/15

$J_{\text{CP}} = 8.0 \text{ Hz}$), 112.7 (s, Indenyl five-membered ring C_q), 122.4–138.8 (aromatic and olefinic CH). – **16a** (CDCl_3): $\delta = 0.16$ (s, SiCH_3), 28.6 (dd, CH_2P^1 , $^1J_{\text{CP}} = 34.0 \text{ Hz}$, $^3J_{\text{CP}} = 5.5 \text{ Hz}$), 30.0 (dd, CH_2P^2 , $^1J_{\text{CP}} = 39.0 \text{ Hz}$, $^3J_{\text{CP}} = 4.1 \text{ Hz}$), 31.4 (s, $\text{CH}_2\text{Indenyl}$), 55.4 (dd, $C_q\text{CH}_2\text{O}$, $^2J_{\text{CP}} = 7.8 \text{ Hz}$ and 4.1 Hz), 58.9 (s, $C_q\text{CH}^4$), 73.9 (t, $C_q\text{CH}_2\text{O}$, $^3J_{\text{CP}} = 13.0 \text{ Hz}$), 75.9 (d, CH^5 , $^2J_{\text{CP}} = 13.6 \text{ Hz}$), 97.5 (s, CH^6), 113.4 (m, $C_q\text{CH}^5$), 117.0 (s, CH^9), 118.0 (s, $C_q\text{CH}^9$), 125.3 (s, CH^6), 125.6 (s, CH^7), 128.2 (s, CH^8), 127.6–143.0 (aromatic CH). For designation of protons see Figure 6. – **16b** (CDCl_3): $\delta = 0.0$ (s, SiCH_3), 7.8 (d, PCH_2CH_3 , $^2J_{\text{CP}} = 32.1 \text{ Hz}$), 8.0 (d, PCH_2CH_3 , $^2J_{\text{CP}} = 26.6 \text{ Hz}$), 15.9 (d, PCH_2CH_3 , $^1J_{\text{CP}} = 21.1 \text{ Hz}$), 25.7 (d, PCH_2CH_3 , $^1J_{\text{CP}} = 24.8 \text{ Hz}$), 28.4 (m, CH_2PEt_2), 29.1 (m, CH_2PPh_2), 30.3 (s, $\text{CH}_2\text{Indenyl}$), 54.7 (dd, $C_q\text{CH}_2\text{O}$, $^2J_{\text{CP}} = 6.4 \text{ Hz}$ and 3.7 Hz), 57.8 (s, $C_q\text{CH}^4$), 71.8 (d, CH^5 , $J_{\text{CP}} = 12.8 \text{ Hz}$), 73.8 (pt, $C_q\text{CH}_2\text{O}$, $^3J_{\text{CP}} = 12.8 \text{ Hz}$), 94.1 (s, CH^4), 116.2 (m, $C_q\text{CH}^5$, $J_{\text{CP}} = 3.7 \text{ Hz}$ and 4.5 Hz), 118.5 (s, CH^9), 119.4 (m, $C_q\text{CH}^9$, $J_{\text{CP}} = 2.7 \text{ Hz}$ and 4.5 Hz), 124.7 (s, CH^6), 125.2 (s, aromatic CH), 126.0 (s, CH^7), 128.5–141.9 (aromatic CH and CH^8). For designation of protons see Figure 9.

$^3\text{P}\{^1\text{H}\}$ NMR: **15a** (CDCl_3): Main product: $\delta = 23.3$ (d, $^2J_{\text{PP}} = 41.0 \text{ Hz}$), 43.2 (d, $^2J_{\text{PP}} = 41.0 \text{ Hz}$). – Minor product: 25.5 (d, $^2J_{\text{PP}} = 39.9 \text{ Hz}$), 40.4 (d, $^2J_{\text{PP}} = 39.9 \text{ Hz}$). – **15b** (CDCl_3): $\delta = 35.7$ (d, $^2J_{\text{PP}} = 35.5 \text{ Hz}$), 40.0 (d, $^2J_{\text{PP}} = 35.5 \text{ Hz}$).

X-ray Crystallographic Study: Suitable crystals were taken directly out of the mother liquor, immersed in perfluorinated polyether oil and fixed to a glass capillary at 200 K. The measurements were carried out with a Nonius–Kappa CCD diffractometer (low-temperature unit, graphite-monochromated $\text{Mo-}K_\alpha$ radiation). The data was processed by the standard Nonius software.^[30] All calculations were performed using the SHELX software package.^[31] Structures were solved by direct methods with the SHELXS-97 programme^[31a] and refined with the SHELXL-97 programme.^[31b] Graphic handling of the structural data during solution and refinement was performed with XPMA.^[32] Atomic coordinates and anisotropic thermal parameters of the non-hydrogen atoms were refined by full-matrix least-squares calculations. Data for the structure determinations are compiled in Table 12. The figures of the structures (Figure 1–3) were made with WinRay-32.^[33] Crystallographic data (excluding structure factors) for the structures reported in this paper have been deposited with the Cambridge Crystallographic Data Centre as supplementary publication no. CCDC-140087 (**7**), -140086 (**anti-8**) and -140088 (**15a**). Copies of the data can be obtained free of charge on application to CCDC, 12 Union Road, Cambridge CB2 1EZ, UK [Fax: (internat.) + 44-1223/336-033; E-mail: deposit@ccdc.cam.ac.uk].

Acknowledgments

We are indebted to the German Science Foundation (DFG), SFB 247, the VW Foundation (Stiftung Volkswagenwerk) and the Fonds der Chemischen Industrie for financial support. A generous loan of ruthenium(III) chloride by the DEGUSSA AG is gratefully acknowledged. We wish to thank T. Jannack (mass spectrometry), the Microanalytical Laboratory and the Mass spectrometry department (high resolution mass spectra) of the Institute of Organic Chemistry.

- Antelmann, U. Winterhalter, G. Huttner, B. C. Janssen, J. Vogelgesang, *J. Organomet. Chem.* **1997**, 545–546, 407–420.
- [3] [3a] B. Antelmann, G. Huttner, U. Winterhalter, *J. Organomet. Chem.* **1998**, 555, 119–125. – [3b] B. Antelmann, G. Huttner, J. Vogelgesang, O. Walter, U. Winterhalter, *J. Organomet. Chem.* **1997**, 549, 139–148.
- [4] [4a] J. Karas, G. Huttner, K. Heinze, P. Rutsch, L. Zsolnai, *Eur. J. Inorg. Chem.* **1999**, 405–420. – [4b] J. Scherer, G. Huttner, M. Büchner, *Chem. Ber.* **1996**, 129, 697–713. – [4c] J. Scherer, G. Huttner, M. Büchner, J. Bakos, *J. Organomet. Chem.* **1996**, 129, 45–58. – [4d] H. Brunner, A. Sicheneder, *Angew. Chem.* **1988**, 100, 730–731; *Angew. Chem. Int. Ed. Engl.* **1988**, 27, 718–719.
- [5] T. Seitz, A. Muth, G. Huttner, *Z. Naturforsch., Teil B* **1995**, 50, 1045–1049.
- [6] B. Antelmann, G. Huttner, U. Winterhalter, *J. Organomet. Chem.* **1998**, 553, 433–441.
- [7] T. Seitz, Ph. D. Dissertation, University of Heidelberg, **1994**.
- [8] H. Heidel, Ph. D. Dissertation, University of Heidelberg, **1994**.
- [9] K. L. Gibis, Ph. D. Dissertation, University of Heidelberg, **1994**.
- [10] L. H. Pignolet, D. Forster, W. d. W. Horrocks, *Inorg. Chem.* **1968**, 7, 828–830.
- [11] [11a] T. Seitz, A. Asam, G. Huttner, O. Walter, L. Zsolnai, *Z. Naturforsch., Teil B* **1995**, 50, 1287–1306. – [11b] T. Seitz, A. Muth, G. Huttner, T. Klein, O. Walter, M. Fritz, L. Zsolnai, *J. Organomet. Chem.* **1994**, 469, 155–162.
- [12] P. Schober, R. Soltek, G. Huttner, L. Zsolnai, K. Heinze, *Eur. J. Inorg. Chem.* **1998**, 1407–1415.
- [13] [13a] K. L. Marsi, M. E. Co-Sarno, *J. Org. Chem.* **1977**, 42, 778–781. – [13b] K. Issleib, H. M. Möbius, *Chem. Ber.* **1961**, 94, 102–106.
- [14] [14a] G. Jany, R. Fawzi, M. Steimann, B. Rieger, *Organometallics* **1997**, 16, 544–550. – [14b] B. Rieger, G. Jany, M. Steimann, R. Fawzi, *Z. Naturforsch.* **1994**, 49b, 451–458. – [14c] B. Rieger, G. Jany, R. Fawzi, M. Steimann, *Organometallics* **1994**, 13, 647–653. – [14d] B. Rieger, G. Jany, *Chem. Ber.* **1994**, 127, 2417–2419. – [14e] B. Rieger, *J. Organomet. Chem.* **1991**, 420, C17–C20.
- [15] K. Urtel, A. Frick, G. Huttner, L. Zsolnai, P. Kircher, P. Rutsch, E. Kaifer, A. Jacobi, *Eur. J. Inorg. Chem.* **2000**, 33–50.
- [16] [16a] U. Piantini, O. W. Sørensen, R. R. Ernst, *J. Am. Chem. Soc.* **1982**, 104, 6800–6801. – [16b] M. Rance, O. W. Sørensen, G. Bodenhausen, G. Wagner, R. R. Ernst, K. Wüthrich, *Biophys. Res. Commun.* **1983**, 117, 479–485.
- [17] B. M. Trost, B. Vidal, M. Thommen, *Chem. Eur. J.* **1999**, 5, 1055–1069.
- [18] [18a] S. Beyreuther, J. Hunger, S. Cunsakis, T. Dierks, A. Frick, E. Planker, G. Huttner, *Eur. J. Inorg. Chem.* **1998**, 1641–1653. – [18b] S. Beyreuther, A. Frick, J. Hunger, G. Huttner, B. Antelmann, P. Schober, R. Soltek, *Eur. J. Inorg. Chem.*, in press.
- [19] J. Jeener, B. H. Meier, P. Bachmann, R. R. Ernst, *J. Chem. Phys.* **1979**, 71, 4546–4563.
- [20] [20a] Felix 98, Molecular Simulations Inc., <http://www.msi.com>. – [20b] Insight II 98.0, Molecular Simulations Inc., <http://www.msi.com>.
- [21] [21a] A. E. Torda, W. F. v. Gunsteren, in *Reviews in Computational Chemistry*, vol. III (Eds.: A. E. Torda, W. F. V. Gunsteren), VCH Publishers Inc., New York, **1996**, chapter 3 and references therein. – [21b] J. M. Blaney, J. S. Dixon, in *Reviews in Computational Chemistry*, vol. V (Eds.: A. E. Torda, W. F. V. Gunsteren), VCH Publishers Inc., New York, **1996**, chapter 6 and references therein.
- [22] A. Bax, M. F. Summers, *J. Am. Chem. Soc.* **1986**, 108, 2093–2094.
- [23] *Organikum*, Deutscher Verlag der Wissenschaften, Berlin, **1990**.
- [24] J. Baldwin, A. Raab, K. Mensler, B. Arison, D. McClure, *J. Org. Chem.* **1978**, 43, 4876–4878.
- [25] K. Issleib, A. Tzschach, *Chem. Ber.* **1959**, 92, 704–711.
- [26] [26a] R. E. Ireland, D. M. Walba, *Org. Synth. Coll. Vol.* **1988**, 6, 567–570. – [26b] K. Issleib, H. O. Fröhlich, *Z. Naturforsch., Teil B* **1959**, 14, 349–350.
- [27] P. S. Hallmann, T. A. Stephenson, G. Wilkinson, *Inorg. Synth.* **1970**, 12, 237–240.
- [28] B. A. Borgias, M. Gachin, D. Kerwood, T. L. James, *Progr.*

[1] S. Martin, H. H. Brintzinger, *Inorg. Chim. Acta* **1998**, 280, 189–192, and references cited therein.

[2] [2a] J. Vogelgesang, G. Huttner, E. Kaifer, P. Kircher, P. Rutsch, S. Cunsakis, *Eur. J. Inorg. Chem.* **1999**, 2187–2199. – [2b] B.

- NMR Spectrosc.* **1990**, 22, 83–100.
- [29] M. Reggelin, H. Hoffmann, M. Köck, D. F. Mierke, *J. Am. Chem. Soc.* **1992**, 114, 3272–3277.
- [30] *DENZO-SMN, Data processing software*, Nonius, **1998**, <http://www.noniuss.com>.
- [31] [31a] G. M. Sheldrick, *SHELXS-97, Programme for Crystal Structure Solution*, University of Göttingen, **1997**, <http://shelx.uni-ac.gwdg.de/shelx/index.html>. – [31b] G. M. Sheldrick, *SHELXL-97, Programme for Crystal Structure Refinement*, University of Göttingen, **1997**, <http://shelx.uni-ac.gwdg.de/shelx/index.html>. – [31c] *International Tables for X-ray Crystallography*, vol. 4, Kynoch Press, Birmingham, U.K., **1974**.
- [32] L. Zsolnai, G. Huttner, *XPMA*, University of Heidelberg, **1994**, <http://www.uni-heidelberg.de/institute/fak12/AC/huttner/htmlsoftware.html>.
- [33] R. Soltek, G. Huttner, *WinRay-32*, University of Heidelberg, **1998**, <http://www.uni-heidelberg.de/institute/fak12/AC/huttner/htmlsoftware.html>.

Received March 3, 2000
[I00240]